

# Dealiasing of Doppler spectra for cloud radar at 94 GHz

Additional thesis  
Peiyuan Wang



# Dealiasing of Doppler spectra for cloud radar at 94 GHz

by

Peiyuan Wang

Student Number

5457653

Instructor: Christine Unal, José Dias Neto  
Project Duration: October, 2022 - February, 2023  
Faculty: Faculty of Civil Engineering, Delft

# Contents

<b>Nomenclature</b>	<b>ii</b>
<b>1 Introduction</b>	<b>1</b>
1.1 Basics about radar	1
1.2 Mean Doppler velocity (MDV) and Aliasing	2
1.3 Range-Doppler dilemma	3
1.4 Previous methods of dealiasing radar measurements	3
<b>2 Data and noise removal</b>	<b>5</b>
2.1 Data description	5
2.1.1 An example of data	6
2.2 Removal of spectral noise	7
<b>3 Method</b>	<b>8</b>
3.1 Basic steps of repairing spectra	8
3.1.1 Unfolding	8
3.1.2 Dealiasing	9
3.2 Reference choice during dealiasing	9
3.2.1 Procedure	9
3.2.2 Initial Reference	10
3.2.3 Filtering out reliable lowest height bins (FRL)	11
3.2.4 Dealiasing upwards	12
3.2.5 Recursion	13
3.2.6 Window Scanning	13
3.2.7 Using neighboring hours to obtain new references	14
<b>4 Result</b>	<b>16</b>
4.1 Unfolded and Dealiased spectrum	16
4.2 Mean Doppler Velocity (MDV)	18
4.2.1 Effect of Dealiasing upwards	18
4.2.2 Effect of Recursion	19
4.2.3 Effect of window scanning	20
4.2.4 Effect of using neighboring hours as reference	21
<b>5 Discussion</b>	<b>22</b>
5.1 Noise removal and unfolding	22
5.2 The difficulty in finding reliable lowest bins (FRL)	23
5.2.1 Common cases	23
5.2.2 More challenging cases	24
5.3 Limitation and Recommendation	24
5.4 Conclusion	25
<b>References</b>	<b>26</b>
<b>A All dealiased <math>V_m</math> on 3rd February, 2021</b>	<b>27</b>
<b>B All dealiased <math>V_m</math> on 18th June, 2021</b>	<b>36</b>
<b>C Inputs and Outputs of the code</b>	<b>45</b>

# Nomenclature

## Frequently used Symbols

Symbol	Definition	Unit
$V_{max}$	Maximum unambiguous Doppler velocity	[m/s]
$V_m$	the mean Doppler velocity of current spectrum	[m/s]
$V_{ref}$	the reference velocity	[m/s]
$V_t$	the true velocity	[m/s]
$v_D$	measured Doppler velocity	[m/s]
$dv$	the velocity resolution	[m/s]
$v_p$	the projected wind velocity	[m/s]
$\rho_{co}$	Co-polar correlation coefficient	

# 1

## Introduction

### 1.1. Basics about radar

A radar emits electromagnetic waves and receives the reflected signal to acquire information about targets. The radar equation describes different contribution of the power returning to the receiving antenna of a radar  $P_r$ :

$$P_r = \frac{P_t G_t A_r \sigma_b F^4}{(4\pi)^2 R^4} \quad (1.1)$$

where  $P_t$  is transmitted power,  $G_t$  the gain of transmitting antenna,  $A_r$  the effective aperture of the receiving antenna,  $\sigma_b$  the backscattering cross section of the target,  $F$  the pattern propagation factor and  $R$  the distance from the target to the radar [12].

For a spherical particle with diameter  $D$  small compared to radar wavelength  $\lambda$  (within Rayleigh regime), the backscatter cross section can be computed by [5]:

$$\sigma_b \approx \frac{\pi^5 |K|^2}{\lambda^4} D^6 \quad (1.2)$$

where  $K$  is the dielectric factor of the particle,  $D$  the diameter of the particle and  $\lambda$  the radar wavelength.

The volumetric radar cross-section can be considered as the summation of the cross-section of all particles within a radar volume. Thus, the total reflectivity  $\eta$  of spherical particles in a radar volume in Rayleigh regime is computed by [5]:

$$\eta = \frac{\pi^5}{\lambda^4} |K_w|^2 Z_e \quad (1.3)$$

where  $K_w$  is dielectric factor of water and  $Z_e$  the equivalent reflectivity factor [5]:

$$Z_e = \frac{1}{\Delta V} \sum_i D_i^6 \quad (1.4)$$

where  $\Delta V$  is radar resolution volume and  $i$  is the number of spherical particles within  $\Delta V$ .

Many observations of cloud radar and weather radar happen within Rayleigh regime. Therefore, millimeter-wavelength radars have the potential to provide a more sensitive probe of cloud particles ranging from a few micrometers in diameter to precipitating drops than radar with longer wavelength (Equation 1.2) [4]. The operating frequency of 94 GHz provides great sensitivity to detect small cloud droplets and thin cirrus (a kind of ice cloud at high altitude) [8]. It also fulfills the need for a compact, low-power and reliable radar system [4], since the backscattering from small targets (relative to rain-drops) such as cloud particles increases proportionally to  $\lambda^{-4}$  (Equation 1.2). The  $\lambda^{-4}$  improvement at 94 GHz is 40 dB with respect to X-band and 17 dB with respect to Ka-band [9]. However, 94 GHz radar also has more challenges. Besides stronger attenuation effect than radars working with longer wavelength [11], the Doppler spectrum obtained will have larger chance suffering from aliasing.

## 1.2. Mean Doppler velocity (MDV) and Aliasing

The mean Doppler velocity  $V_m$  of a spectrum is computed using the equation below,

$$V_m = \frac{1}{P_{tot}} \int vS(v)dv \quad (1.5)$$

where  $v$  is velocity,  $S(v)$  the Doppler power spectrum and  $P_{tot}$  the total power of the spectrum:

$$P_{tot} = \int S(v)dv \quad (1.6)$$

To measure Doppler velocity, it is known that the motion of a target causes a frequency shift and therefore a change in phase in radar signal. The Doppler velocity of a target is acquired by two consecutive measurements of the phase ([5],section 3.4.3).

$$\frac{\partial \varphi}{\partial t} = -2k_0 \frac{\partial r}{\partial t} = -2k_0 v_D \quad (1.7)$$

where  $\varphi$  is the measured phase,  $k_0$  the angular wave number,  $r$  the range, and  $v_D$  the Doppler velocity.

Since the maximum phase shift between two consecutive measurements is  $\pm\pi$ , with Equation 1.7 one can conclude that the maximum Doppler velocity that can be detected by radar is ([5],section 3.6):

$$V_{max} = \pm \frac{\lambda}{4T_0} \quad (1.8)$$

where  $T_0$  is the time between two samples and  $V_{max}$  the maximum unambiguous Doppler velocity.

If the target moves faster than  $V_{max}$ , the phase change will exceed  $\pm\pi$ , aliasing will happen and velocity measurement  $v_D$  will become ([5],section 7.4.5):

$$v_D = V_t + 2nV_{max} \quad (1.9)$$

where  $V_t$  is true Doppler velocity and  $n$  is an integer not equal to zero.

The shape of a Doppler spectrum of  $Z_e$  is often a large peak. The Doppler spectrum would be affected by aliasing. The part of spectrum that is larger than  $V_{max}$  will show up on the other side of the spectrum (Figure 1.1). The mean Doppler velocity will also be affected by aliasing. In Figure 1.1,  $V'_m$  and  $V_m$  are the MDV of true spectrum and aliased spectrum.  $V_{min}$  and  $V_{max}$  are minimum Doppler velocity and maximum Doppler velocity.  $V_{min} = -V_{max}$ .

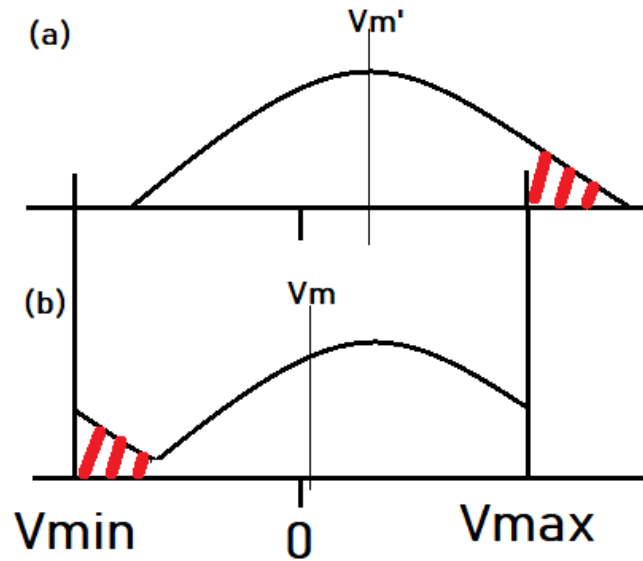


**Figure 1.1: Aliasing:** The red shadowy part of the spectrum is affected by aliasing and therefore misplaced. (a): The true spectrum. (b): Aliased spectrum.

### 1.3. Range-Doppler dilemma

The maximum range that a radar can detect is dependent on the sampling interval  $T_0$  ([5],section 3.6).

$$R_{max} = \frac{cT_0}{2} \quad (1.10)$$

where  $c$  is the speed of light and  $R_{max}$  is the maximum range of radar. Therefore a higher sampling rate can result to larger maximum range of radar. Together with Equation 1.8, one can conclude that ([5],section 7.2):

$$|V_{max}|R_{max} = \frac{c\lambda}{8} \quad (1.11)$$

A radar works on a certain frequency, and thus the multiplication of  $R_{max}$  and  $|V_{max}|$  is a constant for a radar. Consequently, for a radar with shorter wavelength,  $V_{max}$  is reduced to have a similar range compared to radar using a longer wavelength. Comparing  $V_{max}$  from X-band (3 cm wavelength), Ka-band (35 GHz, 9 mm wavelength) with the  $V_{max}$  from W-band (94 GHz, 3mm wavelength) reveals that the  $V_{max}$  of W-band is 10 and 3 times smaller than  $V_{max}$  of the X-band and Ka-band radar system, respectively.

### 1.4. Previous methods of dealiasing radar measurements

There are different types of methods for dealiasing. Methods based on spatial and temporal continuity are quite common ([2, 6, 7]) because they don't require radar to have special working mode. Known velocity information is used as reference to dealias Doppler spectrum. In this process the mean Doppler velocity is used to compare with the reference. In many old studies, the mean Doppler velocity but not spectrum is acquired from radar. Michael and Steven [6] proposed a two-dimensional method. The aliased bins are identified by large spectrum width or low signal-to-noise ratio (SNR), other bins are considered valid (not aliased). Then in the first step, valid velocity of preceding neighbour along the radial is used as reference. 9 neighbors' average can also be used. If there's no enough neighbors found, the algorithm search along the radial to find a closest reference. Velocity Azimuth Display (VAD) will be used as a last option of reference. This method also needs several error detection to correct potential mistakes. Curtis et al.[7] developed a four-dimensional dealiasing algorithm for scanning Doppler radar. This algorithm is a good example of combining temporal and spatial continuity to achieve real-time dealiasing. After noise removal and filtering to remove isolated points, an initial dealiasing is performed using temporal and vertical continuity of mean Doppler velocity. Those successful points

are used as reference to spatial dealiasing, when their neighbors are being dealiased. The accepting threshold of spatial continuity will be relaxed after several passes. The remaining uncorrected points are subjected to window dealiasing, when the average of their neighborhood corrected points is used. Finally, VAD data is used if some aliased points still left.

Another method utilizes staggering pulse repetition time (PRT) technique [5], which relies on changing PRT to modify  $V_{max}$  and  $R_{max}$  in Equation 1.11 to obtain a larger  $V_{max}$  for a certain range. The polarimetric information from radars with linear depolarization ratio (LDR) mode can also be used to dealias [13].

With spectrum data, M. Maahn and P. Kollias [10] triple the Doppler spectrum range and use equivalent reflectivity factor  $Z_e$  to estimate the averaged fall velocity in radar volume for rain and cloud, and use it as a reference to dealias.

The 94-GHz cloud radar used for this study doesn't have a hardware supporting staggering PRT technique or LDR mode, further the radar may look slantwise with the Doppler velocity being not only related to the mean fall velocity, but also to the radial component of the horizontal wind, thus  $Z_e$  cannot be used. Therefore the investigated dealiasing method will use spatial and temporal continuity. In this report, chapter 2 describes data and pre-processing, chapter 3 describes the designed method for dealiasing, chapter 4 shows some typical result of this method and chapter 5 discusses some key issues related to the method.

# 2

## Data and noise removal

### 2.1. Data description

The radar used in this study is the dual-frequency polarimetric scanning cloud radar, CLARA (Cloud Atmospheric Radar) located at atmospheric station in the national Ruisdael Observatory, Cabauw (Figure 2.1 left). It's working with 35 GHz and 94 GHz at the same time. With 35 GHz frequency, a significantly larger range of Doppler velocity is provided, which is a nice approach to validate the dealiasing result of 94 GHz data. Detailed description of the part working at 94 GHz is provided in a paper about an equivalent radar, JOYRAD-94 [8]. Since there are other radars only work at 94GHz (Figure 2.1 right), a dealiasing method for 94GHz radar without relying on 35GHz data is needed.

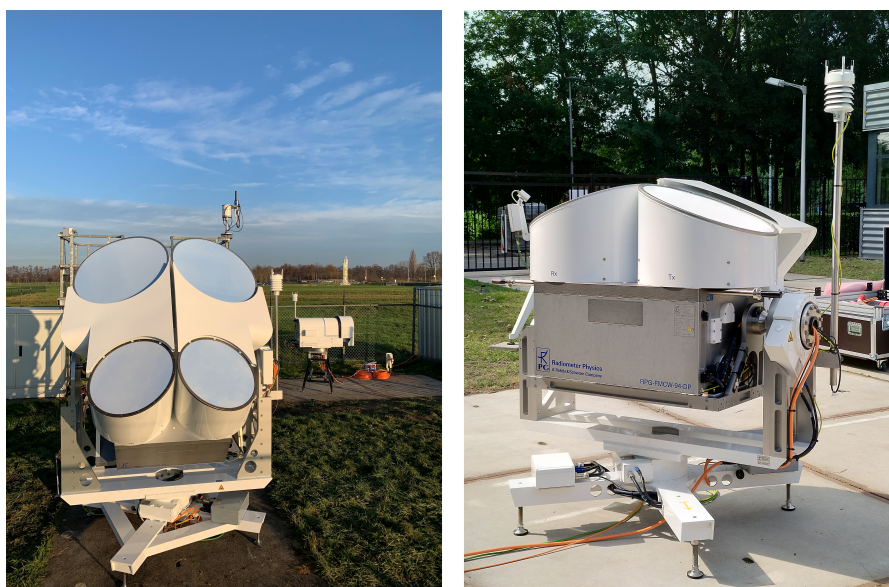


**Figure 2.1:** Left: CLARA at Cabauw. Two lower antennas are 94GHz and two upper ones are 35GHz. Right: The 94GHz radar equivalent to the 94GHz part of CLARA.

There're two level of data product from radar. LV0 products contain Doppler spectrum at horizontal and vertical polarization as well as covariance spectrum, while LV1 products contain mean Doppler velocity, correlation coefficient, differential phase shift and differential reflectivity. A LV0 file is produced each hour by the radar. Under current setting, the Doppler velocity resolution  $dv$  and FFT size  $N$  (the number of bins used for dividing the window of signal into equal strips) is different in three different layers in height as shown in Table 2.1. During its operation, the azimuth angle and elevation angle of the radar are fixed. That means the MDV profile is two-dimensional, time vs. height. The spectra of

HH polarization are used for all the content in this report.

	Chirp 1	Chirp 2	Chirp 3
FFT size	256	256	128
height intervals [m]	84-843	864-3458	3503-10587
range resolution [m]	29.81	29.81	55.04
Maximum Doppler velocity [m/s]	7.35	5.99	3.97
Doppler velocity resolution [m/s]	0.0576	0.0470	0.0625

**Table 2.1:** Parameters setting of the radar

The 24-hour data used in designing this dealiasing algorithm was taken on 3rd February, 2021. There was stratified precipitation in most hours on that day, which provides a lot of connection with ground reference of wind speed. The wind speed at different time didn't change very rapidly during this period, according to  $V_m$  profile from 35GHz radar (Appendix A). The data on 18th June, 2021 is also used for further testing the algorithm. There's a thunderstorm on that day according to weather record, and wind vector changed rapidly (Appendix B). The elevation angle of radar is set as  $45.01^\circ$  on both days.

The wind information near surface is measured by a weather station on the radar. The wind speed and wind direction are recorded synchronously with radar measurement and therefore convenient to use.

### 2.1.1. An example of data

An equivalent reflectivity factor profile  $Z_e$  from 14:00 to 15:00 on 3rd February, 2021 is shown below in Figure 2.2. Stratiform precipitation occurs during this period. Overall  $Z_e$  increases towards the ground with a rapid increase of  $Z_e$  at around 1000m, indicating that the ice particles are melting at this height. The rain below 1000m has strong reflectivity. From cloud top to about 1000m, the  $Z_e$  increases from about  $-20dB$  to about  $0dB$ . From melting layer to the ground, the  $Z_e$  increases from about  $10dB$  to about  $20dB$ . The Figure 2.2 (b) shows strong aliasing of MDV which can't be inferred from Figure 2.2 (a). There are many cycles of velocity value and a sudden jump of velocity between Chirp 2 and Chirp 3 at about 3500 meters.

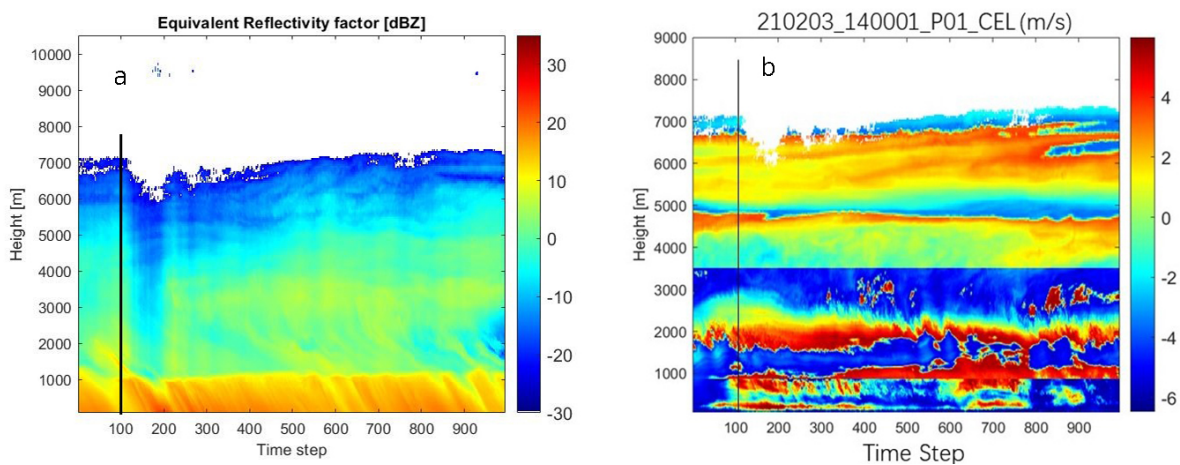


**Figure 2.2:** (a)  $Z_e$  profile from 14:00 to 15:00 on 3rd February, 2021. (b) original  $V_m$  profile at the same time. The black line represents the time of spectrogram that is shown below in Figure 2.3.

The spectrogram at time step 100 shows clear aliasing in Figure 2.3. The spectrum width decreases as height increases in this case. The spectrum width is significantly larger in rain than those above melting layer. From about 700m to 200m, more than one peak exists in the spectrum.

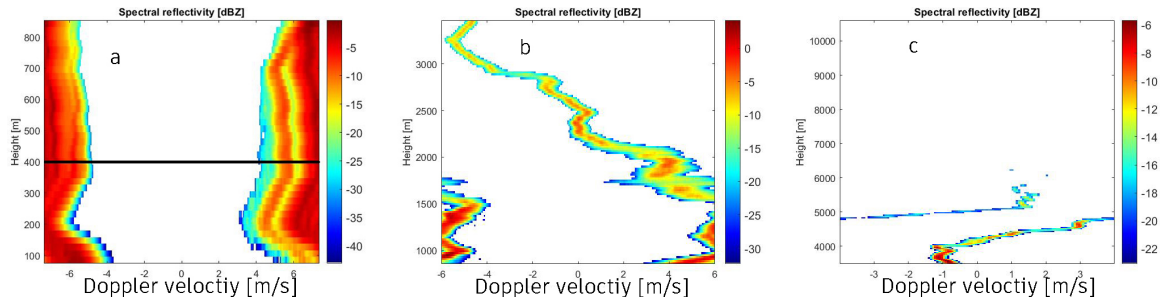


**Figure 2.3:** (a) Spectrogram for Chirp 1, (b) Spectrogram for Chirp 2, (c) Spectrogram for Chirp 3 at time step 100. The black line represents the height of spectrum that is shown in Figure 2.4.

At 400m height, the spectrum is split into two parts (Figure 2.4), and the spectral power between them is removed considering noise level. There are several subpeaks in the spectrum.

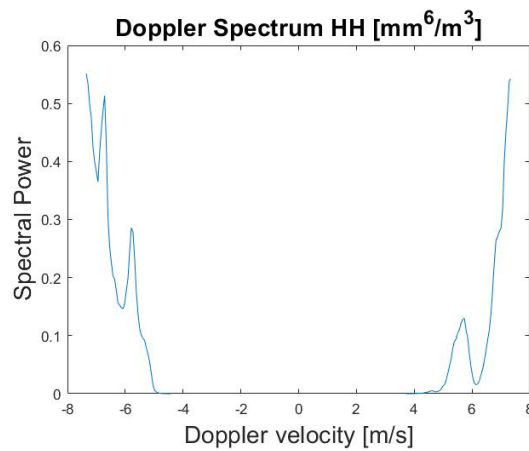


**Figure 2.4:** The spectrum at 400m at time step 100.

## 2.2. Removal of spectral noise

The removal of spectral noise can be applied to the data before dealiasing. That means spectrum with power below a certain value plus the spectral noise power (which is included in LV0 product) is replaced with NaN. This certain value is often set as  $10dB$ . This process will reduce temporal and spatial continuity of Doppler spectrum and makes dealiasing challenging, but it's needed in unfolding. This will be explained in subsection 3.1.1.

In many steps of the algorithm, copolar correlation coefficient  $\rho_{co}$  is used to retain height bins with good data quality (high SNR). The reason is that a high-quality bin is expected to have high  $\rho_{co}$  value because the correlation would decrease significantly due to noise, though a height bin in a melting layer can also have low  $\rho_{co}$ . It's common for  $\rho_{co}$  to be larger than 0.9 outside the melting layer.

# 3

## Method

The prerequisite for this deliasing method (section 3.2) to work is that there's precipitation between cloud and ground during the period that input files cover. Two basic steps of repairing spectrum (unfolding and dealiasing) is firstly described in section 3.1, which is from previous work of Patrick Brukx [3]. This part is repeatedly used in the algorithm. Then the procedure and techniques to find velocity reference are described in section 3.2, which is the main work of the author. Note that all the 'bin' and 'height bin' refer to time-height bin in the following text.

### 3.1. Basic steps of repairing spectra

#### 3.1.1. Unfolding

When spectrum is aliased, sometimes the part that is outside Doppler velocity range will appear on the other end of the spectrum, just as Figure 3.1 (a) shows. Unfolding is needed to repair this kind of spectrum. The method used for unfolding is described in ([3], section 2.1.2).

If the values at both ends of a Doppler spectrum is valid (not a NaN), the spectrum will be unfolded. Otherwise the spectrum will be kept original.

In unfolding, a copy of the spectrum is placed at the left of the original spectrum to get a prolonged spectrum (2N) (Figure 3.1 (b)), N being the FFT size. The middle of the longest sequence of NaN (which is called minimum point) is found in the original spectrum as well as its copy, and the sequence between two minimum points (N) in prolonged spectrum is the result of the unfolding process. Notice that in Figure 3.1,  $V_{min} = -V_{max}$ .

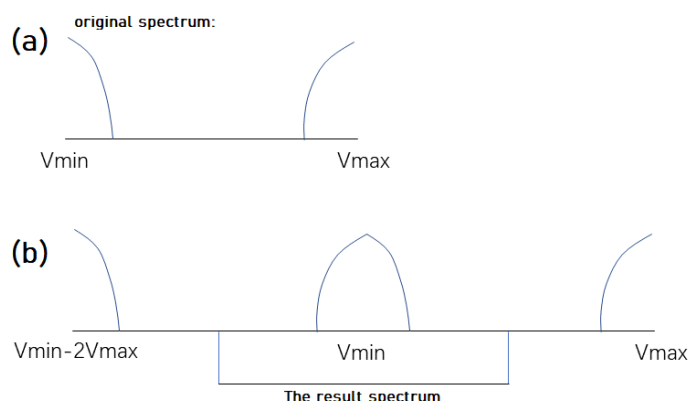


**Figure 3.1: Unfolding:** (a) Original aliased spectrum. (b) A copy of the spectrum is placed at the left of the original spectrum to get a prolonged spectrum.

In some cases, there can be no NaN in some spectrum even after spectral noise removal such as

the case in section 5.1. To prevent failure of unfolding under such circumstances, a value need to be chosen and spectral power below this value can be considered as NaN sequence in unfolding. This value should not be too large in case too much useful spectrum is removed and continuity is damaged. Therefore, if there's still no sequence equivalent to NaN, the smallest 5% of the spectrum value is regarded as NaN sequence.

### 3.1.2. Dealiasing

To determine the value of  $n$  in Equation 1.9, the MDV  $V_m$  of unfolded spectrum is computed using Equation 1.5 and compared with a reference velocity  $V_{ref}$ . The choice of reference  $V_{ref}$  will be discussed in section 3.2.

To compute  $n$  which can make  $V_t$  within the range of  $(V_{ref} - V_{max}, V_{ref} + V_{max})$  in Equation 1.9, it is known that,

$$-V_{max} \leq V_m - V_{ref} < V_{max} \quad (n = 0) \quad (3.1)$$

$$(-2n - 1)V_{max} \leq V_m - V_{ref} < (-2n + 1)V_{max} \quad (n \in N^+) \quad (3.2)$$

$$(-2n - 1)V_{max} \leq V_m - V_{ref} < (-2n + 1)V_{max} \quad (n \in Z^-) \quad (3.3)$$

So once  $(V_m - V_{ref})/V_{max}$  is computed,  $n$  can also be solved.

For example in Figure 3.2,  $V_{ref}$  is within the range between  $V_m + V_{max}$  and  $V_m + 3V_{max}$ , which means

$$V_m + V_{max} < V_{ref} \leq V_m + 3V_{max} \quad (3.4)$$

$$-3V_{max} \leq V_m - V_{ref} < -V_{max} \quad (3.5)$$

and therefore,

$$-2n - 1 = -3 \quad (3.6)$$

$$n = 1 \quad (3.7)$$

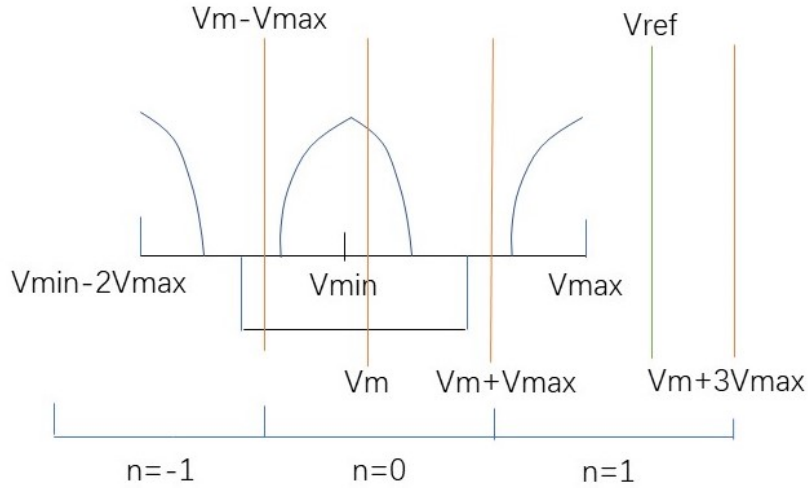


**Figure 3.2: Dealias:** This figure gives an example of the implementation of Equations 3.1 - 3.3. The  $V_{ref}$  is shown in green line, and value of  $n$  is shown at the bottom.  $n$  is determined when  $V_{ref}$  falls in one of those ranges of  $n$ .

## 3.2. Reference choice during dealiasing

### 3.2.1. Procedure

To start with, all the lowest height bins are dealiased using horizontal wind measurements as reference. Then all the bins from lowest to top are dealiased for every time step. Since there can be measurements

with low SNR near radar which can lead to wrong results in higher bins, careful selection is needed in these processes.

Afterwards, recursion and window scanning can be used to tackle remaining bins. The result of previous and following hours can also be used as reference. These methods will be discussed in following sections.

The whole procedure is shown below.

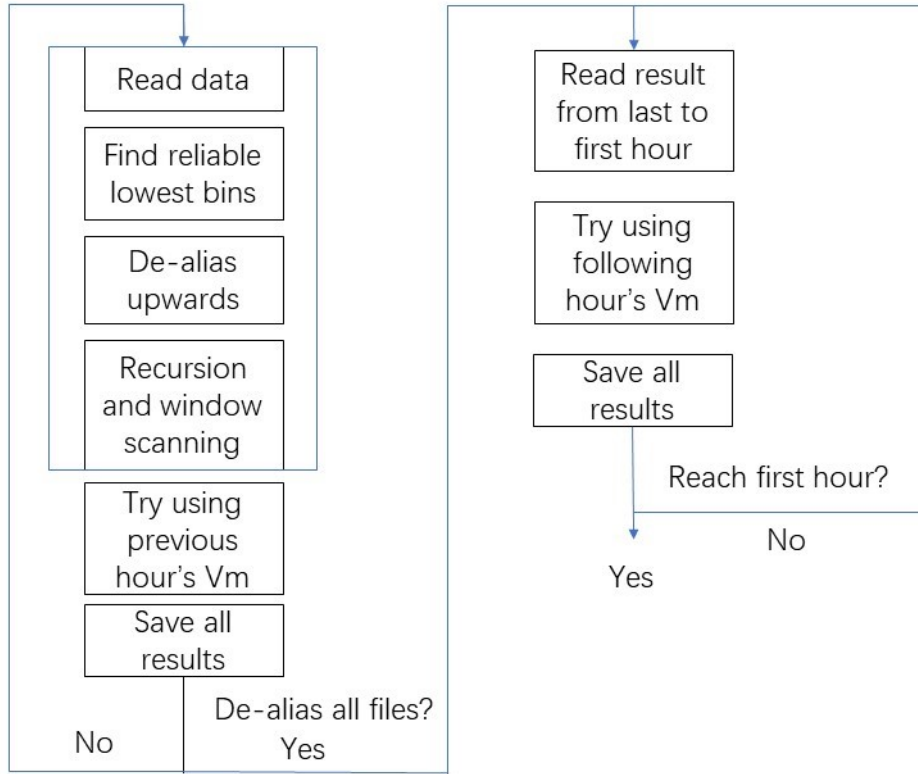


**Figure 3.3: Procedure of the entire algorithm:** The spectra is read from the first to the last hour and several methods are used to dealias. Results from previous hours and following hours are also used as reference in such an order shown.

To dealias Doppler spectrum for clouds that don't rain in a hour but rain in previous or following hours, a procedure is designed as Figure 3.3. Detailed description of this is provided in subsection 3.2.7.

### 3.2.2. Initial Reference

The horizontal wind (speed and direction) measured by the weather station on the radar can provide the initial reference to dealias the Doppler spectrum. It is measured along with radar measurement at each time step.

The horizontal wind vector needs to be projected into the pointing direction of the radar. The projected wind vector  $v_p$  is computed as,

$$v_p = v_H \cos\alpha \cos(D - \phi \pm \pi) \quad (3.8)$$

where  $\alpha$  is the radar elevation angle,  $D$  the horizontal wind direction related to the North,  $v_H$  the horizontal wind speed and  $\phi$  the radar azimuth direction. But in our data, the provided horizontal wind direction is,

$$D' = D \pm \pi \quad (3.9)$$

therefore,

$$v_p = v_H \cos\alpha \cos(D' - \phi) \quad (3.10)$$

### 3.2.3. Filtering out reliable lowest height bins (FRL)

The lowest height bins for all time steps are dealiased at first, using projected wind speed from weather station. This result can contain some mistakes because of the uncertain relationship between horizontal wind vector at ground level and at the lowest height bin. These mistakes can lead to the oscillation of dealiased  $V_m$  of lowest height bins shown in Figure 5.3 and the effect in Figure 3.4, which will be discussed. A procedure to find out reliable results and make some correction is designed. Below are the details of the three steps of this procedure:

1. From empirical model of the terminal fall velocities of raindrops, it is known that [1]

$$v_f(D) = 9.65 - 10.3\exp(-0.6D) \quad (3.11)$$

where  $v_f$  is fall velocity of raindrop (m/s),  $D$  is equivolume diameter of raindrop in unit of  $mm$ . Considering that the diameter of a raindrop is larger than  $0.1mm$ , the range of  $v_f$  can be  $[0, 9.65] m/s$ . This can be projected to radar beam knowing the elevation angle and combined with the projected horizontal wind in Equation 3.10. The Doppler velocity near ground is expected to be within

$$[v_p, v_p - 9.65\sin\alpha] (m/s) \quad (3.12)$$

Based on this hypothesis about the fall velocity of raindrops, the  $V_m$  after dealiasing at lowest height bins should be more or less within this range. So the lowest height bins with  $V_m$  after dealiasing that fulfill this criteria are picked as first step. This case is shown in Figure 5.3. Besides, to reduce the effect of noisy bins,  $\rho_{co}$  is required to be larger than  $0.9$  in Chirp 1. This value is empirical.

2. Usually, a mean Doppler velocity of radar volume that is smaller than the projected horizontal wind is expected near the ground due to the negative contribution of the mean raindrop fall velocity. However in some cases, the projected horizontal wind  $v_p$  is not a correct reference for the lowest bin. This can lead to the violation of our hypothesis in step 1 and no reliable lowest height bins can be found (Or finding wrong ones), when the lowest height bins in an hour have dealiased  $V_m$  (blue curve) larger than projected horizontal wind (orange curve, 'prowind') in Figure 3.4. The 'fall' in the figure is  $9.65\sin\alpha$  in Equation 3.12.

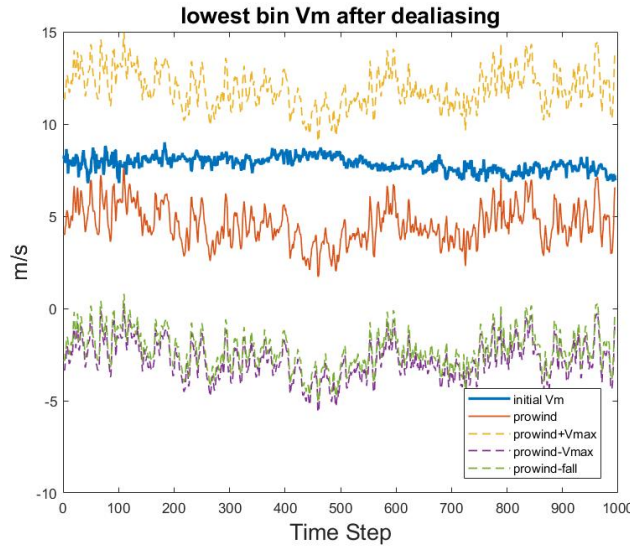


**Figure 3.4:** 19:00 to 20:00 on 3rd Feb, 2021. The blue curve shows initially dealiased  $V_m$  using projected horizontal wind  $v_p$  ('prowind'). The red curve represents the projected horizontal wind. Yellow and purple dash line show the  $\pm V_{max}$  boundary of the projected horizontal wind. Green dash line shows the value of projected horizontal wind minus  $9.65\sin\alpha$ . All the dealiased  $V_m$  of lowest height bins are larger than corresponding projected horizontal wind.

This situation of dealiased  $V_m$  in Figure 3.4 is highly impossible to occur given the negative contribution of  $v_f$  in  $V_m$ . To identify and correct  $V_m$  in this situation, when the standard deviation of

the difference between initially dealiased  $V_m$  (blue curve) and  $v_p$  (red curve) in an hour is smaller than a certain value  $\Delta$ , if

$$V_m(i) > v_p + 0.5V_{max} \quad (3.13)$$

then  $2V_{max}$  is subtracted from  $V_m$ .

$$V_m(i) = V_m(i) - 2V_{max} \quad (3.14)$$

where  $i$  is the time step index.

$\Delta$  is used to limit the use of this operation. The reason is that empirically if the standard deviation is large enough, it's more likely to make mistakes in this operation. Detailed explanation is given in subsection 5.2.2.  $\Delta$  is empirically set as  $2 \text{ m/s}$ . Therefore, misuse of this operation can be strictly limited.

The lowest height bins that are corrected are included in reliable lowest height bins. More discussion of this step and result of the case Figure 3.4 is shown in section 5.2.

3. The standard deviation  $\delta$  and mean  $\overline{V_m}$  of  $V_m$  that passed Step 1 (and Step 2) in one hour is computed. If any  $V_m(i)$  that pass Step 1 (and Step 2) fulfill

$$|V_m(i) - \overline{V_m}| > \delta \quad (3.15)$$

where  $i$  is the time step index. They're deleted from reliable lowest height bins. The purpose is to filter out some extreme values which can be wrong. This step is also empirically necessary.

More detailed discussion can be found in section 5.2.

### 3.2.4. Dealiasing upwards

After having the result  $V_m$  of lowest height bins, an efficient way to dealias other bins is to dealias from lowest to top bins in times steps when precipitation come from cloud to ground. Since every bin uses its lower neighbour's  $V_m$  as reference, all mistakes need to be avoid in case they're transferred to other bins. These mistakes can be due to sudden change of wind vector and noise, which cause abrupt changes of dealiased  $V_m$ . There are two criteria to prevent this:

1. A threshold of co-polar correlation coefficient  $\rho_{co}$  is used to filter out noisy height bins in Chirp 1. It is learned from experience. This value is chosen as 25th percentile of all  $\rho_{co}$  in Chirp 1 in an hour.
2. The dealiased  $V_m(j)$  and its reference  $V_m(j-1)$  must have

$$|V_m(j) - V_m(j-1)| < 0.5 V_{max} \quad (3.16)$$

where  $j$  is the order of dealiasing shown in Figure 3.5. Since bins that don't fulfill criterion 1 and NaN bins exist, the reference bin can be several bins lower than current bin (Figure 3.5). The distance allowed is set as 7 bins, but this can vary according to weather condition. The value 7 is a conservative criterion here. If criterion 2 is not fulfilled, dealiasing further upwards will be given up and move on to next time step. The 0.5 in Equation 3.16 is an empirical value. If a larger value is used, some errors may not be filtered out. If a smaller value is used, less bins will be dealiased in this step.

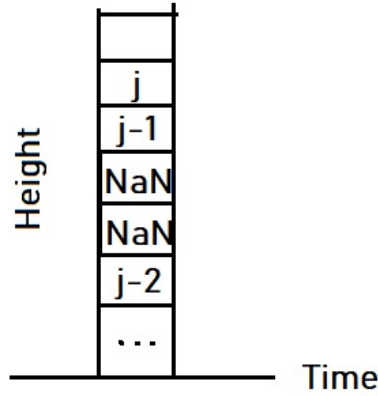


**Figure 3.5: Dealiasing upwards:** NaN height bins will be skipped.  $j$  is the order of dealiasing

If the gap between the reference bin and current bin is too large, dealiasing further upwards will also be given up and move on to next time step.

### 3.2.5. Recursion

To dealias bins that are connected to dealiased bins, recursion is used. Recursion means using one neighbor as reference to dealias others. The reference is updated if the result  $V_m$  is acceptable:

$$|V_{m,ref} - V_m| < 0.05 V_{max} \quad (3.17)$$

where  $V_{m,ref}$  is the reference velocity from a neighbour height bin. The neighborhood of a height bin is its Moore neighbourhood. The value 0.05 is an empirical value. This value is tested by trying out different values and works effectively. A larger value has high risk of making mistakes, but lower value can cause more aliased height bins left and longer computational time.

This criterion is stricter than in subsection 3.2.4, one reason is that  $\rho_{co}$  criterion is not used here. Also, unlike subsection 3.2.4, the neighbor in recursion is right next to the aliased height bin, and therefore a smaller difference of  $V_m$  between them is expected.

The recursion function continues dealiasing neighbors' neighbors until no more aliased neighbors left or reach maximum recursion depth (The number of levels of activation of this procedure which exist during the deepest call of this procedure). The maximum depth is set as 30000 given the memory of my laptop.

Recursion is used of all height-time bins in every hour, so that it reaches all the height-time bins that are possible to reach. Recursion is more flexible than one-dimensional method such as dealiasing along the height in subsection 3.2.4, but it takes much more memory and time. That's why it's not used right after having reliable lowest height bins result.

### 3.2.6. Window Scanning

The limit of recursion is that it can't reach height bins which are not connected to dealiased bins. That's why this method is also needed.

All the height bins that are not NaN bins and connected by Moore neighborhood are considered as an island, such as the two islands in Figure 3.6. These isolated aliased islands (upper right island in Figure 3.6) of bins can be reached, if they're not too far away (temporally and spatially) from dealiased islands (lower left island in Figure 3.6 with green shadow and cross). The average of dealiased  $V_m$  within the neighborhood (red box) of the aliased bin (the bin with red dot) is computed (Equation 3.18). These dealiased bins are with green cross in Figure 3.6. Then the average velocity is used as the

reference to dealias the bin with red dot. The reference velocity is computed as below:

$$V_{m,ref} = \frac{1}{n} \sum_{i=1}^n V_m(i) \quad (3.18)$$

where  $n$  is the number of dealiasied bins within window.

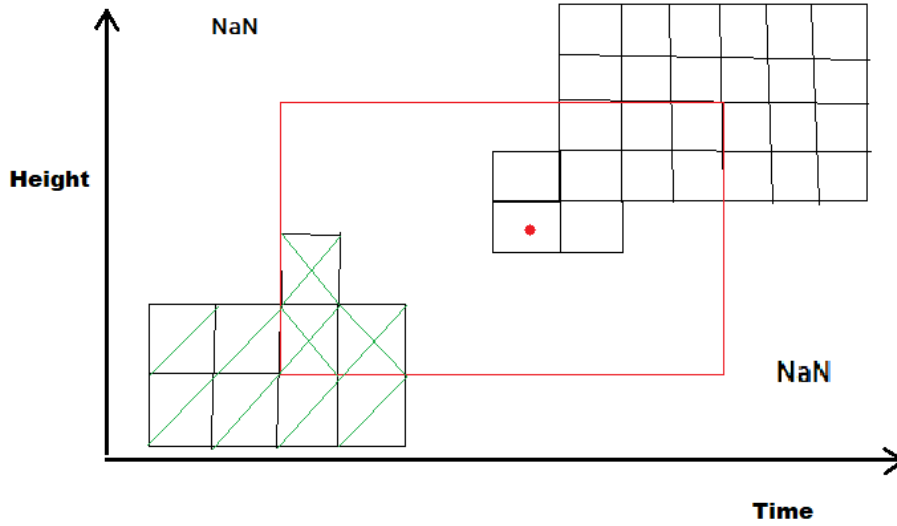


**Figure 3.6: Window scanning:** The average of dealiasied  $V_m$  inside red square box is computed. In this case three bins with green cross are used. Then the aliased bin with red dot can be dealiasied with such a reference. Recursion can completely dealias upper right island with dealiasied  $V_m$  of bin with red dot.

In window scanning process, all aliased height bins are found one by one and the  $V_{ref}$  is computed with the  $V_m$  of dealiasied bins in a window around them. The newly dealiasied  $V_m$  is checked with Equation 3.19. If the criterion is not fulfilled, the result  $V_m$  will be given up.

The window size contains two dimensions: time and space, as our Doppler velocity profile. The window size needs to be set manually according to variability of wind vector in time and space. For example, a smaller window size should be used for a storm case, because the wind changes rapidly and larger window size can lead to wrong reference. To dealias the example data on 3rd February (with relatively stable weather condition), the temporal size is set as 50 bins (about 3 minutes) and spatial size is 10 bins (about 300m in range and 212m in height with radar elevation angle of  $45^\circ$ ).

There's also a similar criterion of acceptance for window scanning:

$$|V_{m,ref} - V_m| < 0.2V_{max} \quad (3.19)$$

$V_m$  here is the dealiasied MDV of an aliased height bin. 0.2 is an input of function so that it can be changed conveniently. This value need to be chosen by considering window size and spatial temporal variability of wind. A larger value will have higher chance to make a error.

Usually, window scanning and recursion are used in turns in order to dealiasied as many bins as possible. This process can be relatively time-consuming.

### 3.2.7. Using neighboring hours to obtain new references

From first hour to last hour, each file is dealiasied as much as possible with methods mentioned before. The dealiasied  $V_m$  of last time step of previous hour is saved and used as reference for next hour if

needed. For the second to last hours, this reference is updated after trying to use previous one. Recursion and window scanning with this reference will be used if there are aliased bins at the first time step. Once no more bins can be dealiased even with reference on the left, aliased bins at last time step is checked and their indexes in  $V_m$  profile are saved in a variable. By doing this, computational time can be saved in later procedure. The dealiased spectra and  $V_m$  profile are also saved for each hour in different mat file (file type of Matlab for storing data).

After that, from last hour to first hour, similar process is used again. If there's aliased bins at last time step in an hour, the mat files of this hour and next hour are loaded. Recursion and window scanning are used. The mat file of this hour will be updated. If there's only one file, only the left part of the procedure in Figure 3.3 is used.

# 4

## Result

*This section will show some intermediate and final results of the algorithm to better present how the algorithm works. The intermediate results include unfolded spectra, the  $V_m$  profile after dealiasing upwards, recursion and window scanning. The final results include dealiased  $V_m$  profile and spectra. All the time axes in figures below are shown in time step rather than the actual UTC time for it's more accurate and easier to validate in the code and data.*

### 4.1. Unfolded and Dealiasied spectrum

An example of a spectrum being unfolded and dealiasied is shown below in Figure 4.1, it's at the 100th time step of 15th hour on 3rd February, 2021. The figures a,a' and a" are from Chirp 3. Figure b, b' and b" are from Chirp 2. Figures c, c', c" are from Chirp 1. They're plotted separately because the FFT size of Chirp 1,2 (256) is different from Chirp 3 (128).

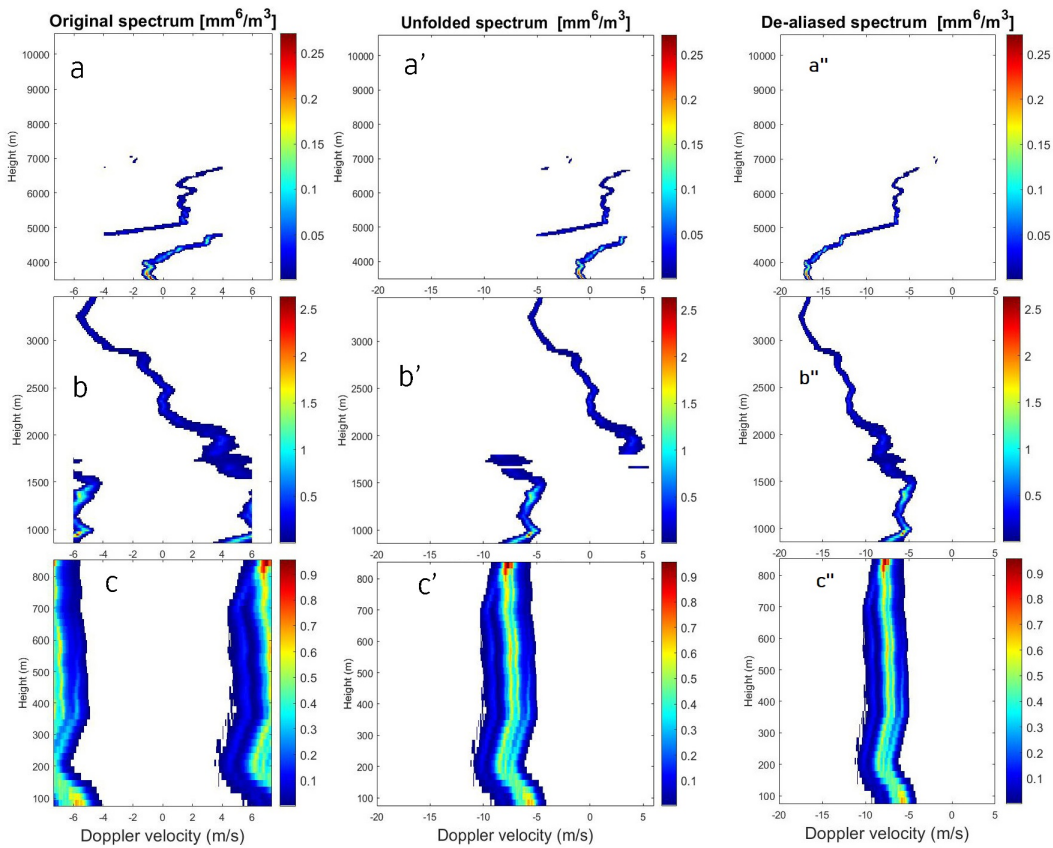


**Figure 4.1:** (a,b,c) original spectra of the 100th time step of 15th hour on 3rd February, 2021. (a',b',c') unfolded spectra of the 100th time step of 15th hour on 3rd February, 2021. (a'',b'',c'') dealiased spectra of the 100th time step of 15th hour on 3rd February, 2021.

Figure 4.1 (a'-c') and Figure 4.1 (a''-c'') shows what unfolding and dealiasing do to the spectrogram. The split, mislocated spectrums are repaired by unfolding and dealiasing. The continuity of the spectrogram is back. In Figure 4.1 (b), it is clear that Chirp 2 has a smaller  $V_{max}$  compared to Chirp 1 (figure (a)). The original MDV profile of this hour is shown in Figure 4.2 with strong aliasing effect. The  $V_m$  of 35GHz (Figure 4.2 (b)) also shows aliasing effect (red part) from about 5000m to about 3000m. The black line in Figure 4.2 (a) (b) is the position of the time step.

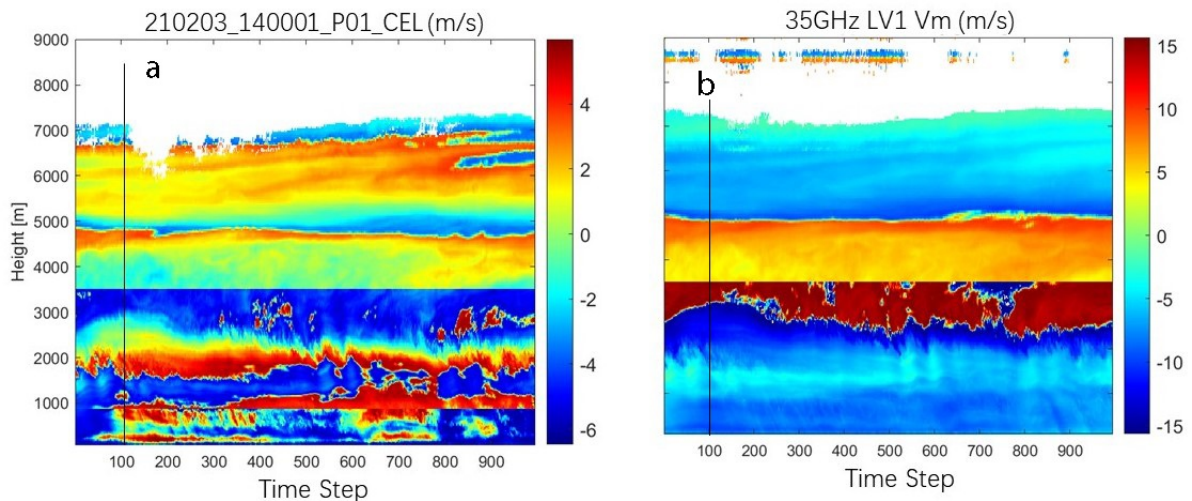


**Figure 4.2:** (a) 94GHz original  $V_m$  at 14:00 to 15:00 on 3rd February, 2021. The black line shows the 100th time step. (b) 35GHz LV1  $V_m$  at the same time

## 4.2. Mean Doppler Velocity (MDV)

The dealiased MDV profile of 15th hour on 3rd February is shown in Figure 4.3 (c) to give an example of dealiased  $V_m$  profile. In this hour continuous precipitation exists, and the variation in wind speed is significant at different height. In Figure 4.3 (c), from 7000m to about 3000m the MDV decreases from about 0m/s to -18m/s. Then MDV increases again towards the ground. Strong aliasing occurs in velocity profile in 94GHz data (Figure 4.3 (a)) and 35GHz data is also partially affected as shown in Figure 4.3 (b).

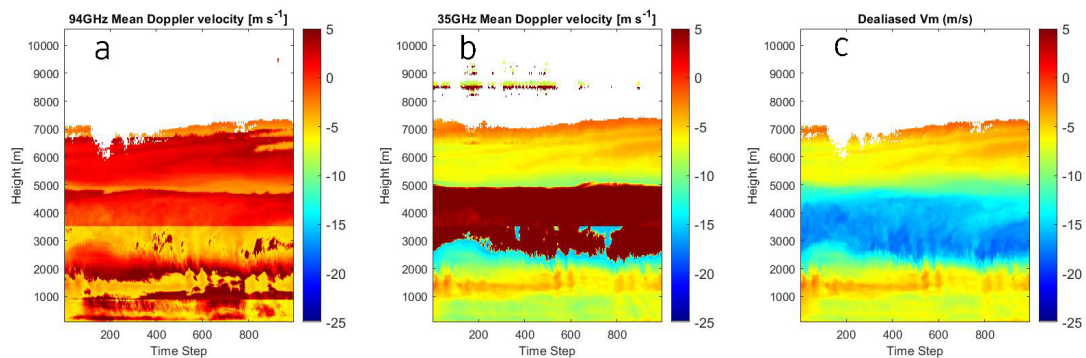


**Figure 4.3:** (a) Original 94GHz  $V_m$  profile. (b) Original 35GHz  $V_m$  profile (dark red part is aliased). (c) Dealiased  $V_m$  profile on 14:00 to 15:00 on 3rd February, 2021

The continuity of velocity profile is repaired, and is consistent with 35GHz LV1 product (though aliasing also happens at mid altitude).

### 4.2.1. Effect of Dealiasing upwards

In a case when MDV profile has good continuity and many lowest height bins are reliable, such as the 14th hour of 3rd February, 2021, dealiasing upwards can produce most part of dealiased MDV profile result. The dealiased MDV profile of this hour after dealiasing upwards is shown below in Figure 4.4 (a). However in other cases, dealiasing upwards will have difficulty in dealiasing more bins, due to lack of continuity of original  $V_m$  profile and reliable lowest height bins (Figure 4.4 (b)).

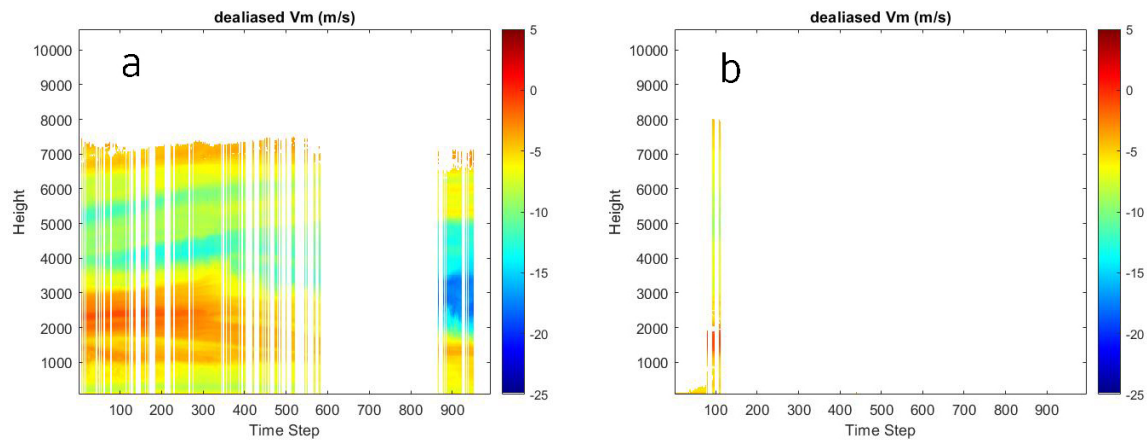


**Figure 4.4:** (a):  $V_m$  on 13:00 to 14:00 on 3rd February, 2021 after dealiasing upwards. (b):  $V_m$  on 18:00 to 19:00 on 3rd February, 2021 after dealiasing upwards.

Another example is the 18th hour on 3rd February in Figure 4.5. Furthermore, the 22nd hour on that day doesn't even have any  $V_m$  profile results because no reliable lowest height bins are acquired.

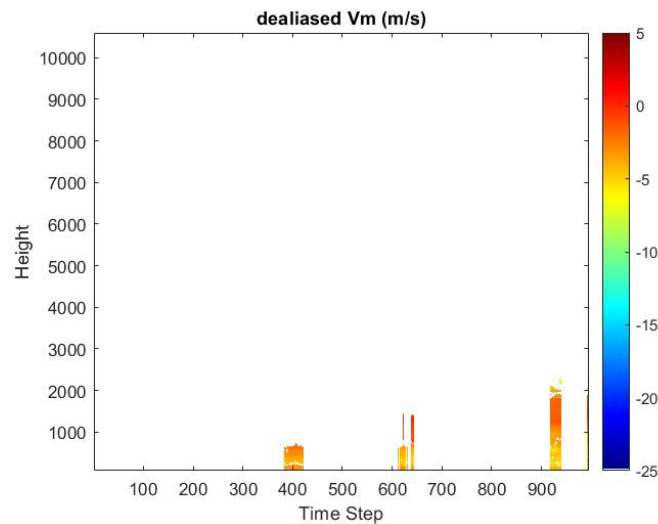


**Figure 4.5:**  $V_m$  on 17:00 to 18:00 on 3rd February, 2021 after dealiasing upwards.

The ratio of the number of dealiased height-time bins and all non-NaN height-time bins (called 'dealiased ratio' for simplicity) is computed for these hours after dealiasing upwards in Table 4.1.

14th hour	19th hour	18th hour	22nd hour
41.65%	1.09%	2.71%	0%

**Table 4.1:** dealiased ratio after dealiasing upwards

#### 4.2.2. Effect of Recursion

Recursion is used based on the result of dealiasing upwards. The dealiased  $V_m$  profile after recursion is shown below:

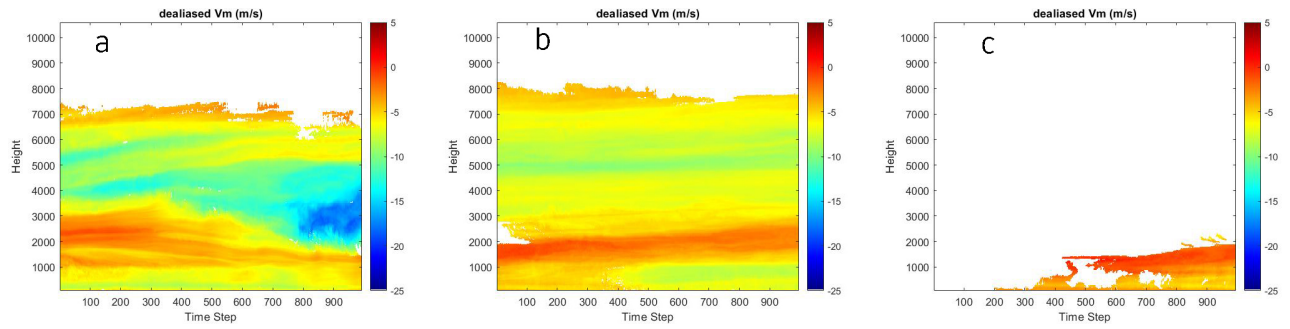


**Figure 4.6:** (a)  $V_m$  from 13:00 to 14:00 on 3rd February, 2021. (Compared with Figure 4.4 (a) ) (b)  $V_m$  from 18:00 to 19:00 on 3rd February, 2021. (Compared with Figure 4.4 (b) ) (c)  $V_m$  from 17:00 to 18:00 on 3rd February, 2021. (Compared with Figure 4.5)

The first two profiles in Figure 4.6 are considered fully dealiased after recursion is used. Their corresponding 35GHz  $V_m$  profile are Figure A.14 and Figure A.19. The upper cloud of the 18th hour cannot be dealiased only using recursion for the lack of continuity of  $V_m$  profile (Figure 4.6 (c) ).

Since no bins are dealiased in 22nd hour, recursion also can't do anything and the dealiased  $V_m$  profile for the 22nd hour is still blank. The dealiased ratio after recursion is shown in Table 4.2. There's significant increase of dealiased ratio on 14th, 19th and 18th hour.

14th hour	19th hour	18th hour	22nd hour
99.87%	99.48%	23.62%	0%

**Table 4.2:** dealiased ratio after recursion

### 4.2.3. Effect of window scanning

The  $V_m$  profile of 18th hour is further dealiased with the help of window scanning (Figure 4.7 (b)), compared to Figure 4.6(c). The upper cloud that has little connection with lower precipitation is dealiased. Window scanning and recursion are used several times to reach the resulting profile. This  $V_m$  profile (18th hour) is considered fully dealiased to this point.

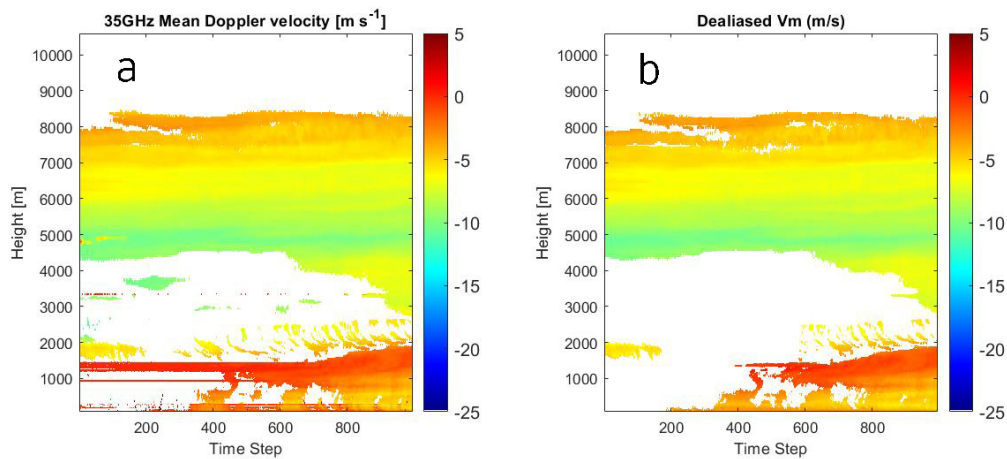


**Figure 4.7:** (a): 35GHz LV1  $V_m$  from 17:00 to 18:00 on 3rd February, 2021. (b)  $V_m$  from 17:00 to 18:00 on 3rd February, 2021.

The dealiased ratio for 18th hour increases from 23.62% to 97.01% after window scanning is used combined with recursion for several times.

#### 4.2.4. Effect of using neighboring hours as reference

To show the effect of using  $V_m$  result from previous hour as reference, the situation of  $V_m$  from 22nd to 24th hour of 3rd Feb is a good case and shown below. The dark red parts of 35GHz  $V_m$  in Figure 4.8 (b) and (c) are aliased, but for 94GHz in Figure 4.9 they're dealiased. The red lines in lower cloud of 35GHz profiles are noise. Some light precipitation reach the ground for lower clouds during this period. Without using  $V_m$  result from previous hour, the upper cloud in last two hours cannot be dealiased.

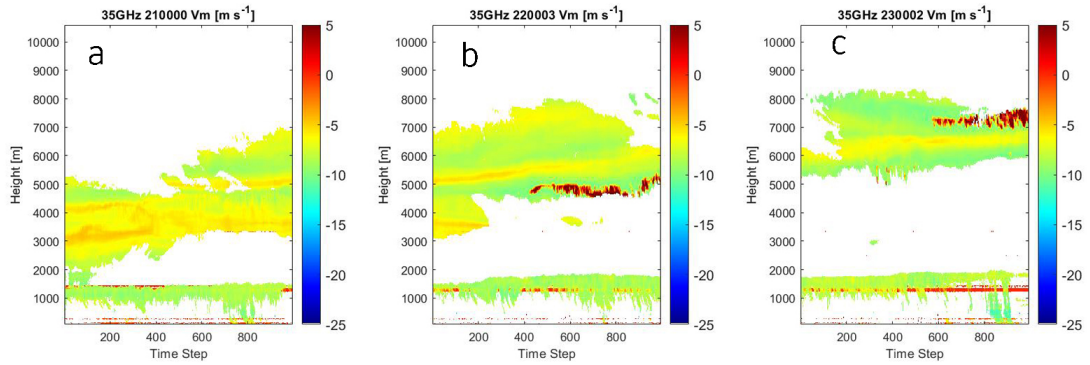


**Figure 4.8:** 35GHz aliased: (a)  $V_m$  on 21:00 to 22:00 on 3rd February, 2021. (b)  $V_m$  on 22:00 to 23:00 on 3rd February, 2021. (c)  $V_m$  on 23:00 to 24:00 on 3rd February, 2021.

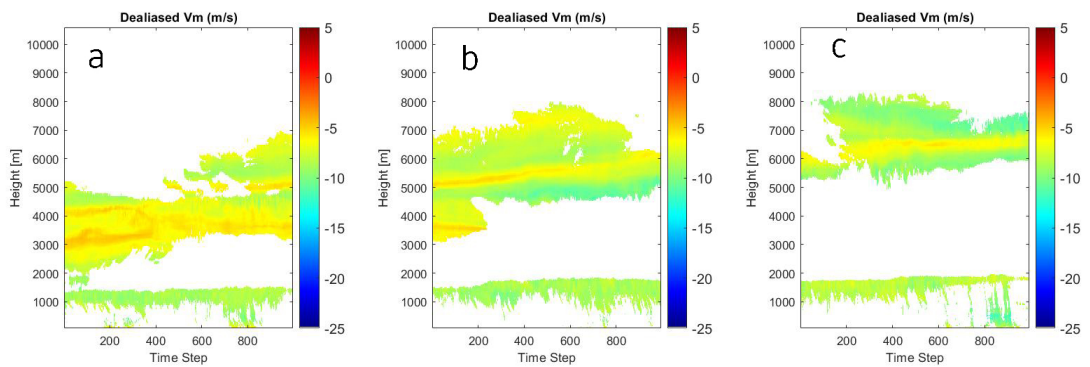


**Figure 4.9:** 94GHz dealiased: (a)  $V_m$  on 21:00 to 22:00 on 3rd February, 2021. (b)  $V_m$  on 22:00 to 23:00 on 3rd February, 2021. (c)  $V_m$  on 23:00 to 24:00 on 3rd February, 2021.

From Figure 4.8 and Figure 4.9, one can conclude that the dealiased ratio for 22nd, 23rd and 24th hour are closed to 100% after using neighboring hours' dealiased MDV.

All the other dealiased  $V_m$  profiles on 3rd February and 18th June, 2021 is shown in Appendix A and Appendix B.

# 5

## Discussion

### 5.1. Noise removal and unfolding

In subsection 3.1.1, it is mentioned that the lowest spectral power of some spectrum is still significantly higher than noise level. These spectra is at relatively high altitude and spectrum width is large, so they overlap at lowest point of spectral power due to aliasing. Thus the noise removal is not helpful for unfolding in this case. This happens in some bins at 16:00 to 18:00 on 18th June, 2021. Two of such spectra are shown in Figure 5.1. Their locations are also shown in Figure 5.2.

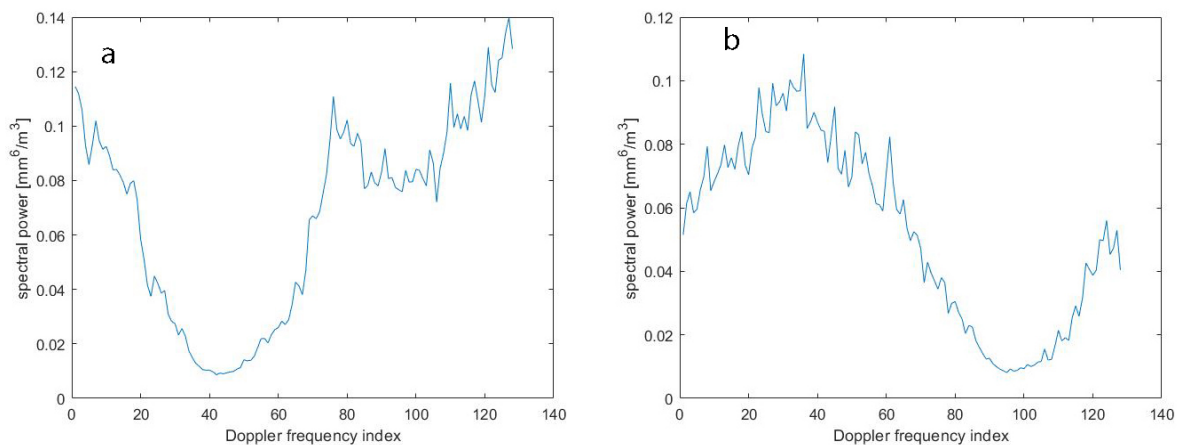


**Figure 5.1:** Two examples of spectra with high spectral power. (a) A case at about 600 time step of 17th hour(16:00-17:00) (b) A case at about 100 time step of 18th hour(17:00-18:00)

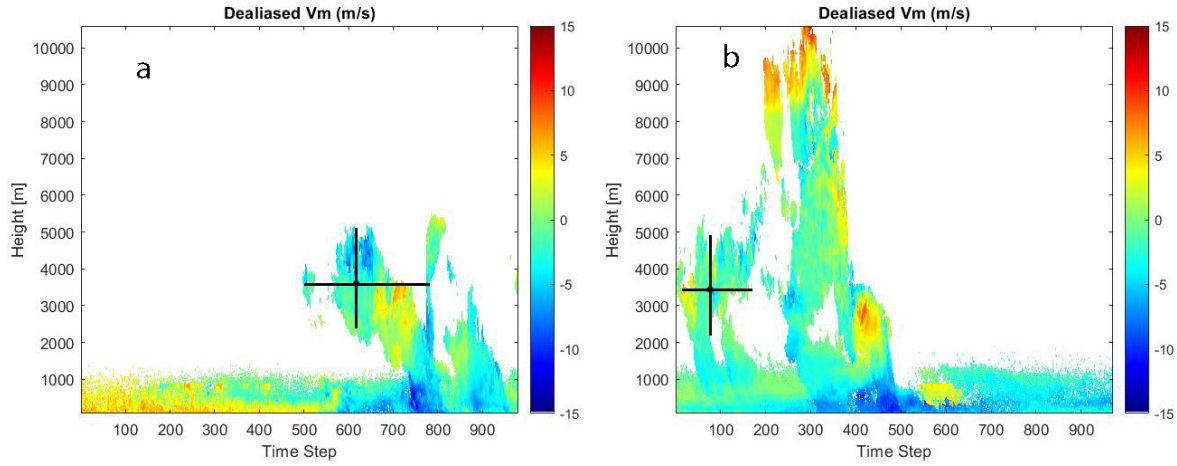


**Figure 5.2:** (a) Dealised  $V_m$  on 16:00 to 17:00 on 18th June, 2021. (b) Dealised  $V_m$  on 17:00 to 18:00 on 18th June, 2021. The locations of these bins are shown at black cross.

The method in subsection 3.1.1 can deal with this situation, since the spectrum is split at correct location. However, the spectrum width and mean Doppler velocity can have some error after dealiasing because the dealiased spectrum is not the same as the real spectrum.

## 5.2. The difficulty in finding reliable lowest bins (FRL)

The relationship between the horizontal wind measured at the surface by the weather station and the horizontal wind at the lowest bin is not known. This is tricky to deal with.

### 5.2.1. Common cases

The most common phenomenon in dealiased  $V_m$  of lowest bins is the oscillation of initially dealiased  $V_m$  (blue curve) shown in Figure 5.3. The reason for this to happen is that the wind at two locations are not changing with same amplitude at the same time. If for example, at a moment  $V_{m,after\ unfolding} - V_{ref} < V_{max}$ , at next time step  $V_{m,after\ unfolding} - V_{ref} > V_{max}$ ,  $n$  solved by dealiasing in subsection 3.1.2 will be different and a velocity difference close to  $2V_{max}$  between two moment will occur.

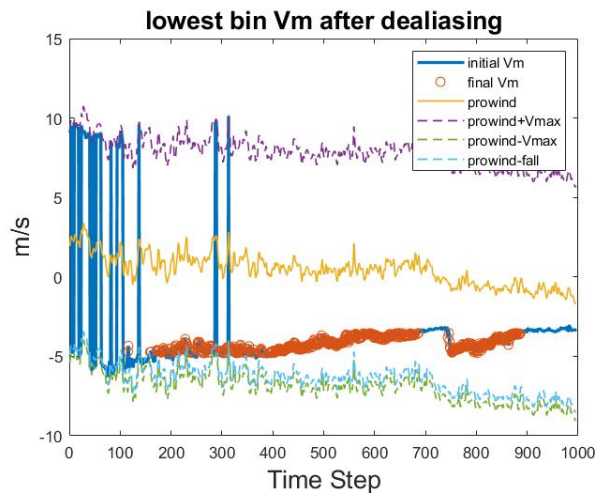


**Figure 5.3:**  $V_m$  of lowest bins versus time (from 15:00 to 16:00 UTC on 3rd February, 2021). The thick blue curve shows the initially dealiased  $V_m$  using projected measured horizontal wind vector  $v_p$  ('prowind'). The yellow curve represents the projected measured horizontal wind vector. Green and purple dash line show the  $\pm V_{max}$  boundaries of the projected horizontal wind vector. Blue dash line shows the projected horizontal wind vector minus  $9.65 \sin \alpha$ . Orange circles show taken reliable lowest bins. Some  $V_m$  in Figure 5.3 meet the criterion of Step 1 in FRL but they're not taken, because their  $\rho_{co}$  is too small. The dealiased  $V_m$  of first 100 time step shows strong oscillation.

The first step in FRL(subsection 3.2.3) is useful in dealing with this oscillation of initially dealiased  $V_m$  which is the most simple case. In Figure 5.3 the bins with orange circles are retained as lowest bin references. The large values in oscillation  $V_m$  is highly impossible to be reliable due to negative contribution of rainfall velocity, and therefore they're removed in step 1 of FRL.

### 5.2.2. More challenging cases

However, the cases similar to Figure 3.4 are challenging. The Step 2 in FRL tries to solve this, based on the fact that initial  $V_m$  is not expected to be stably above projected wind speed if they're correct. 'Stably' means that the initial  $V_m$  doesn't cross projected wind speed (yellow curve in Figure 5.4) and should follow the trend of projected wind speed for some time. Therefore, a result as Figure 5.4 (Orange circle) can be acquired:

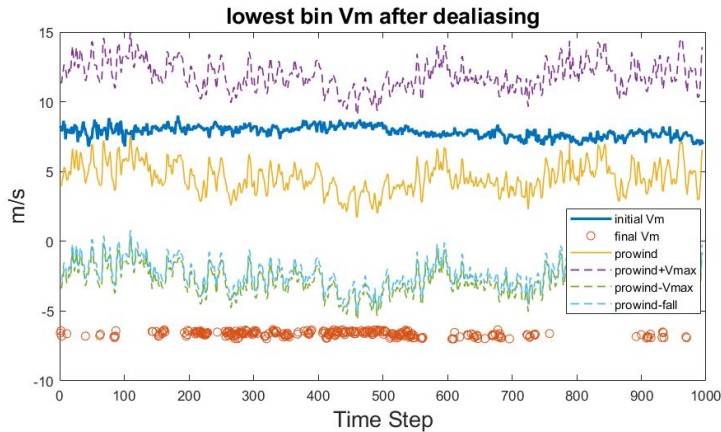


**Figure 5.4:** The result of Figure 3.4. The legend is the same as Figure 5.3. Orange circles show the reliable bins.

One thing worth mentioning is that the value 0.5 in Equation 3.13 works in two days of data I used, but the optimal value can vary when the elevation angle of radar is quite different from  $45^\circ$ . If the elevation angle is larger than  $45^\circ$ , mean raindrop fall velocity will further reduce the value of expected Doppler velocity at the lowest bins, while horizontal wind contribute less in Doppler velocity at the lowest bins. Therefore, there's less chance for a true  $V_m$  that's larger than  $v_p$  to occur and a smaller value rather than 0.5 can be used in Equation 3.13. If the elevation angle is smaller than  $45^\circ$ , the opposite applies.

Due to limited cases I've seen, this mechanism could fail in unexpected cases. Therefore, the criterion  $\Delta$  in Step 2 of subsection 3.2.3 will need to be adjusted manually depending on situation.

## 5.3. Limitation and Recommendation

The proposed method is designed and tested based on relatively few data, and therefore it's possible for unexpected cases to occur and failure happens. That's why several thresholds and criteria need to be set manually according to different cases in future usage. This process can be time-consuming and clear understanding of the code is needed. More works need to be done to make algorithm smarter and convenient to use. For example, the value 0.5 in Equation 3.13 can be replaced with a function of elevation angle. The criterion Equation 3.13 itself can also be replaced if more understanding about this issue is gained. Besides, the window size in window scanning can be decided by the variation of wind vector in time and height direction. Ideally the algorithm should be able to deal with all different cases without human interference.

One limitation of dealiasing 94GHz Doppler spectrum in our case is lack of reliable reference. No matter what methods are designed, accurate and adequate reference is always needed. It can make things much easier compared to current situation. The horizontal wind measurement at the surface is the only source of reference in our case, and we've already seen many difficulties in using it because

(1) it's on the ground and away from all the bins and (2) it's often noisy and affected by more turbulence near surface and (3) it's not enough. In Figure A.6 and Figure A.7, high clouds that are not close to any de-aliased clouds cannot be de-aliased due to lack of reference.

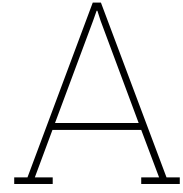
A balance between dealiasing as much bins as possible and correctness is needed when designing methods. Further research can focus on utilizing other sources of reference such as model output from ECMWF as reference to fully dealias clouds without precipitation.

## 5.4. Conclusion

In this study a method for dealiasing spectra of 94 GHz cloud radar with fixed azimuth and elevation angle when precipitation presents on the ground is proposed. A dual-frequency cloud radar is used for designing this algorithm, which allows comparison between the dealiased results at 94GHz with the mean Doppler velocity measured at 35GHz. The method is designed for one frequency only because there is single-frequency radar at 94GHz as well within the Ruisdael Observatory. The spectra of VV polarization can be dealiased similar to spectra of HH polarization, with minor adjustment of parameters. These parameters are not optimal for all cases and need adjustment when applied to new cases. Furthermore, this method can be applied to spectra at 35GHz as well without significant modification. The results include the dealiased MDV profile and dealiased spectra.

# References

- [1] David Atlas, RC Srivastava, and Rajinder S Sekhon. "Doppler radar characteristics of precipitation at vertical incidence". In: *Reviews of Geophysics* 11.1 (1973), pp. 1–35.
- [2] William R Bergen and Steven C Albers. "Two-and three-dimensional de-aliasing of Doppler radar velocities". In: *Journal of Atmospheric and Oceanic technology* 5.2 (1988), pp. 305–319.
- [3] PBJ Brukx. "Dealiasing of radar Doppler velocities to improve wind estimations". In: (2015).
- [4] EE Clothiaux et al. "An evaluation of a 94-GHz radar for remote sensing of cloud properties". In: *Journal of Atmospheric and Oceanic Technology* 12.2 (1995), pp. 201–229.
- [5] Richard J. Doviak and Dusan S. Zrnica (Auth.) *Doppler Radar and Weather Observations*. 2nd ed. Elsevier Inc, Academic Press, 1993. ISBN: 978-0-12-221422-6, 0122214226. URL: <http://gen.lib.rus.ec/book/index.php?md5=47dfefb05ee413c597de17470cad9d9d>.
- [6] Michael D Eilts and Steven D Smith. "Efficient dealiasing of Doppler velocities using local environment constraints". In: *Journal of Atmospheric and Oceanic technology* 7.1 (1990), pp. 118–128.
- [7] Curtis N James and Robert A Houze. "A real-time four-dimensional Doppler dealiasing scheme". In: *Journal of Atmospheric and Oceanic Technology* 18.10 (2001), pp. 1674–1683.
- [8] Nils Kuchler et al. "A W-band radar–radiometer system for accurate and continuous monitoring of clouds and precipitation". In: *Journal of Atmospheric and Oceanic Technology* 34.11 (2017), pp. 2375–2392.
- [9] Roger Lhermitte. "A 94-GHz Doppler radar for cloud observations". In: *Journal of Atmospheric and Oceanic Technology* 4.1 (1987), pp. 36–48.
- [10] M Maahn and P Kollias. "Improved Micro Rain Radar snow measurements using Doppler spectra post-processing". In: *Atmospheric Measurement Techniques* 5.11 (2012), pp. 2661–2673.
- [11] Sergey Y Matrosov. "Potential for attenuation-based estimations of rainfall rate from CloudSat". In: *Geophysical research letters* 34.5 (2007).
- [12] George W Stimson. *Introduction to airborne radar*. SciTech Publishing, Inc., 1998.
- [13] CMH Unal and DN Moiseev. "Combined Doppler and polarimetric radar measurements: Correction for spectrum aliasing and nonsimultaneous polarimetric measurements". In: *Journal of atmospheric and oceanic technology* 21.3 (2004), pp. 443–456.



# All dealiased $V_m$ on 3rd February, 2021

All 24 hours of dealiased  $V_m$  profiles on 3rd February, 2021 are shown below. For comparison, the original  $V_m$  profiles of 35GHz LV1 products are also provided.

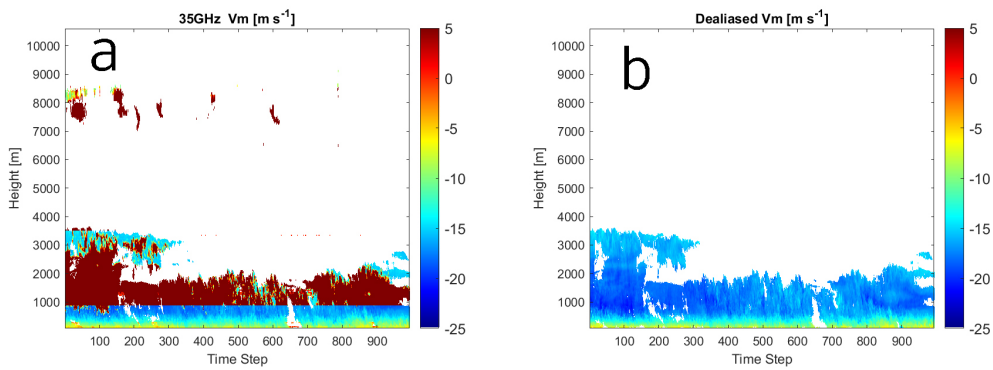


**Figure A.1:**  $V_m$  from 00:00 to 01:00 on 3rd February, 2021. (a) 35GHz LV1 products MDV profile. (b) Dealiased 94GHz MDV profile.

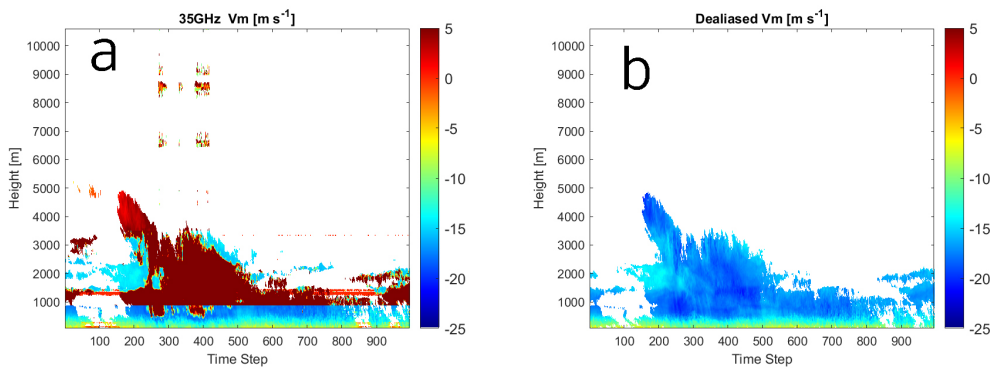


**Figure A.2:**  $V_m$  from 01:00 to 02:00 on 3rd February, 2021. (a) 35GHz LV1 products MDV profile. (b) Dealiased 94GHz MDV profile.

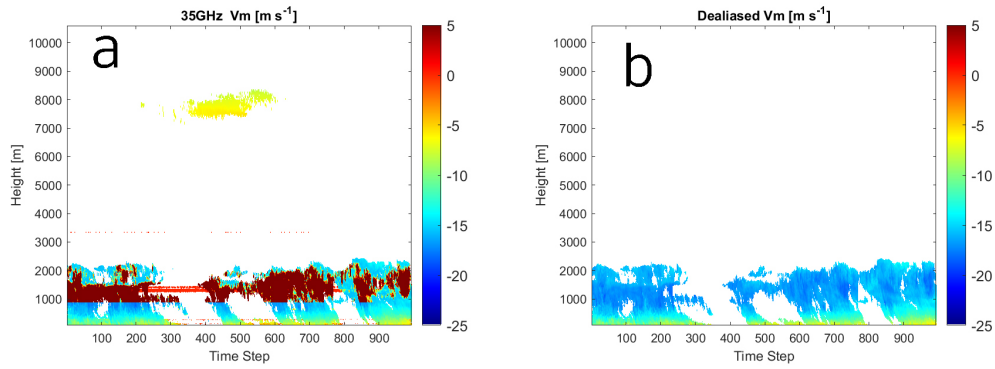


**Figure A.3:**  $V_m$  from 02:00 to 03:00 on 3rd February, 2021. (a) 35GHz LV1 products MDV profile. (b) Dealiased 94GHz MDV profile.

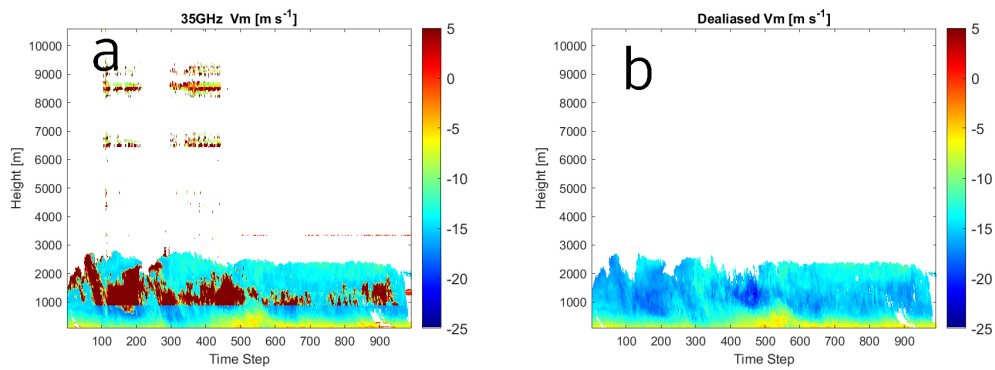


**Figure A.4:**  $V_m$  from 03:00 to 04:00 on 3rd February, 2021. (a) 35GHz LV1 products MDV profile. (b) Dealiased 94GHz MDV profile.

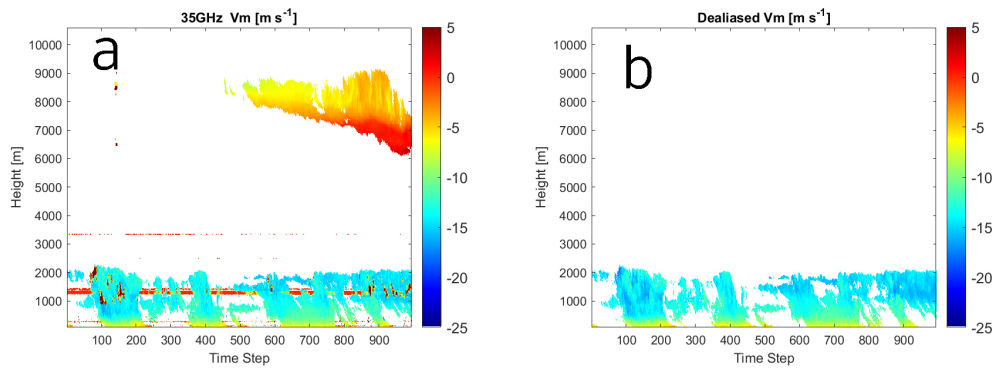


**Figure A.5:**  $V_m$  from 04:00 to 05:00 on 3rd February, 2021. (a) 35GHz LV1 products MDV profile. (b) Dealiased 94GHz MDV profile.

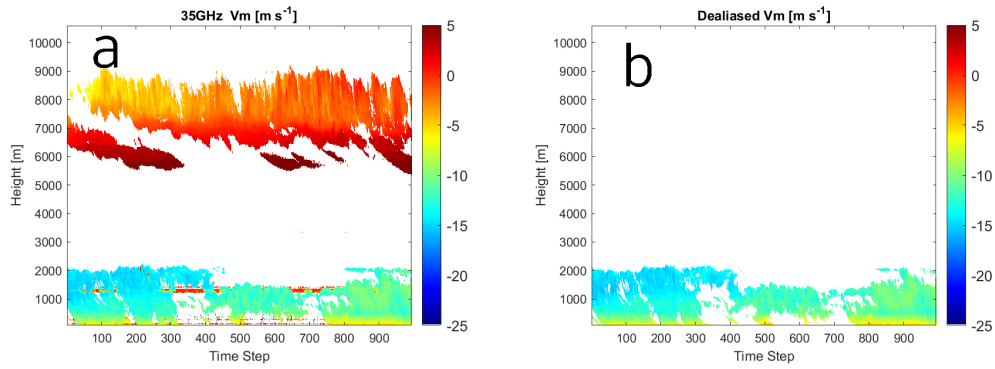


**Figure A.6:**  $V_m$  from 05:00 to 06:00 on 3rd February, 2021. (a) 35GHz LV1 products MDV profile. (b) Dealiased 94GHz MDV profile.

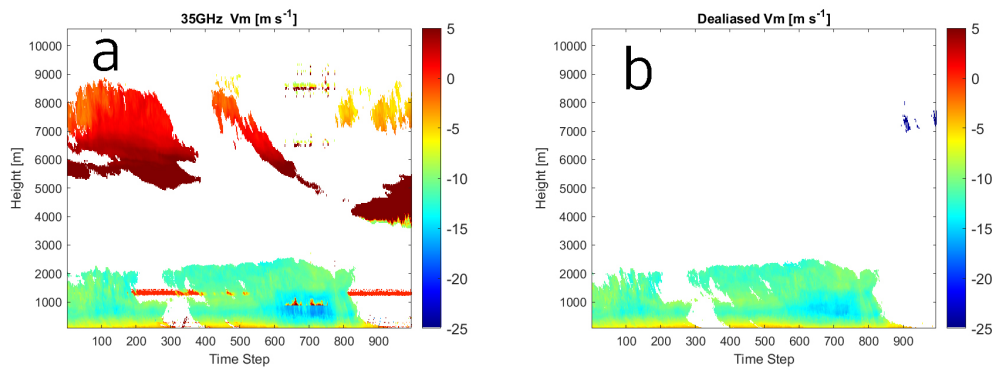


**Figure A.7:**  $V_m$  from 06:00 to 07:00 on 3rd February, 2021. (a) 35GHz LV1 products MDV profile. (b) Dealiased 94GHz MDV profile.

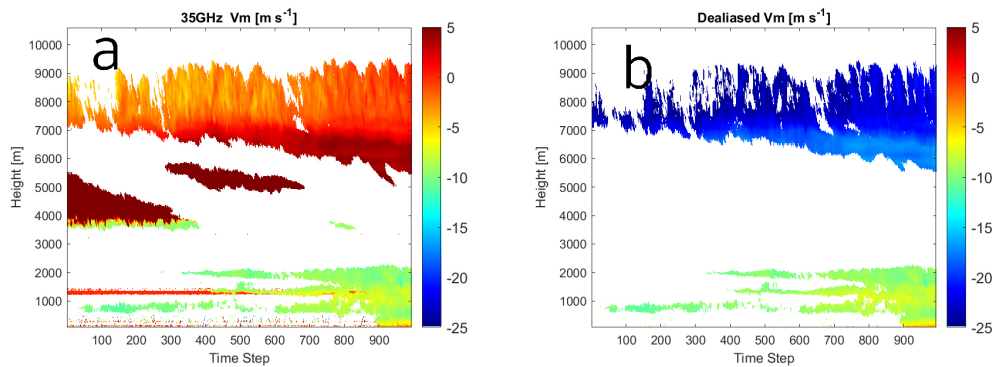


**Figure A.8:**  $V_m$  from 07:00 to 08:00 on 3rd February, 2021. (a) 35GHz LV1 products MDV profile. (b) Dealiased 94GHz MDV profile.

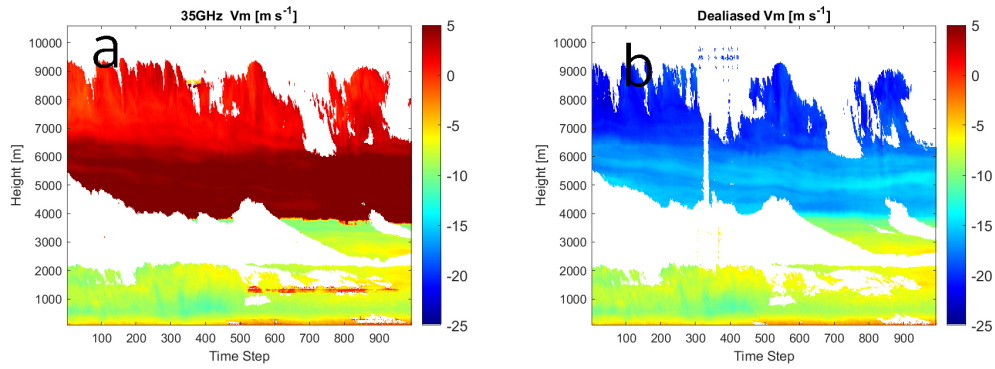


**Figure A.9:**  $V_m$  from 08:00 to 09:00 on 3rd February, 2021. (a) 35GHz LV1 products MDV profile. (b) Dealiased 94GHz MDV profile.

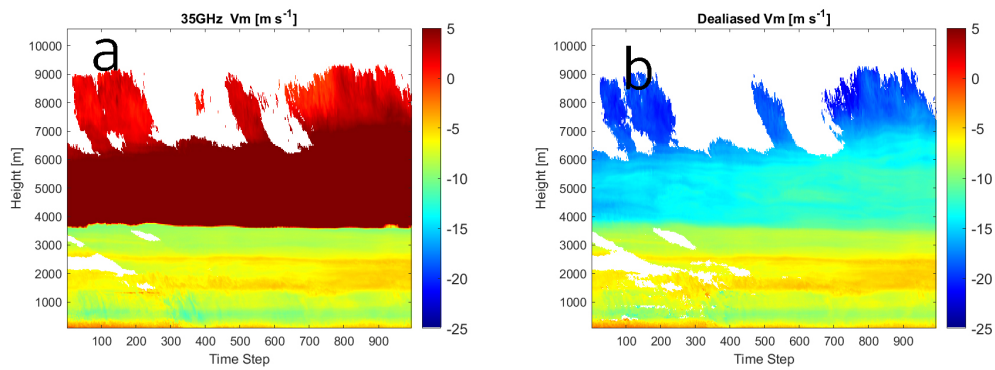


**Figure A.10:**  $V_m$  from 09:00 to 10:00 on 3rd February, 2021. (a) 35GHz LV1 products MDV profile. (b) Dealiased 94GHz MDV profile.

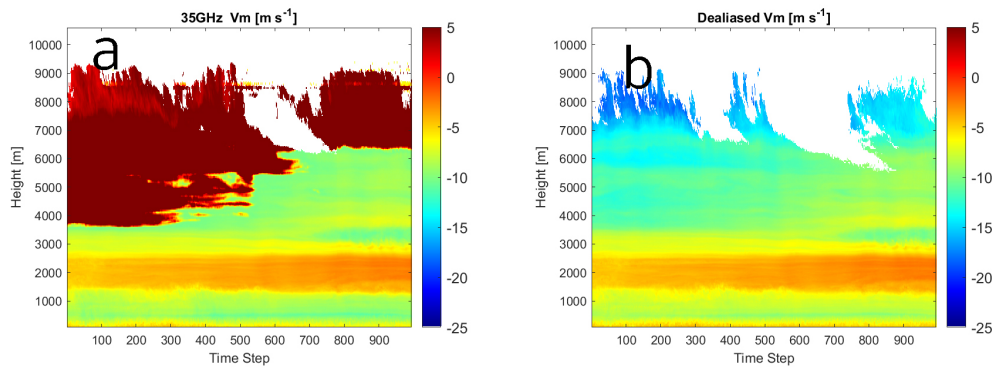


**Figure A.11:**  $V_m$  from 10:00 to 11:00 on 3rd February, 2021. (a) 35GHz LV1 products MDV profile. (b) Dealiased 94GHz MDV profile.

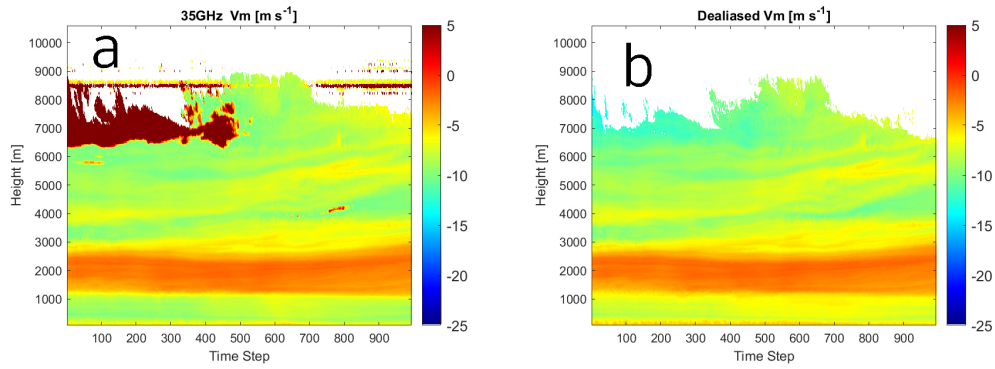


**Figure A.12:**  $V_m$  from 11:00 to 12:00 on 3rd February, 2021. (a) 35GHz LV1 products MDV profile. (b) Dealiased 94GHz MDV profile.

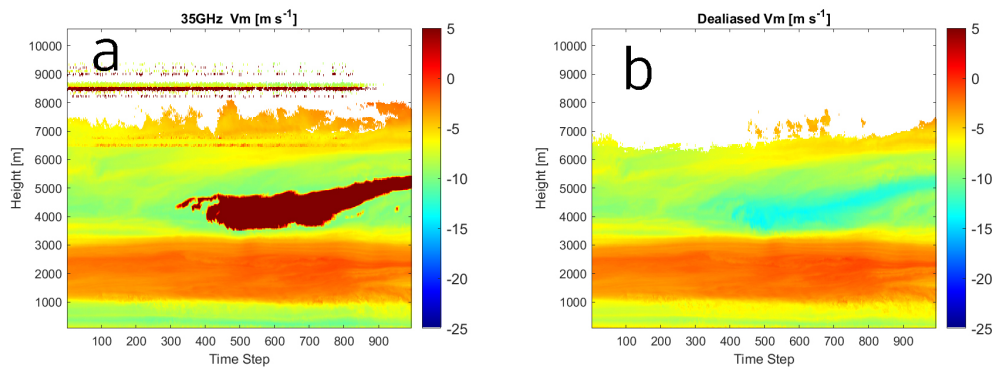


**Figure A.13:**  $V_m$  from 12:00 to 13:00 on 3rd February, 2021. (a) 35GHz LV1 products MDV profile. (b) Dealiased 94GHz MDV profile.

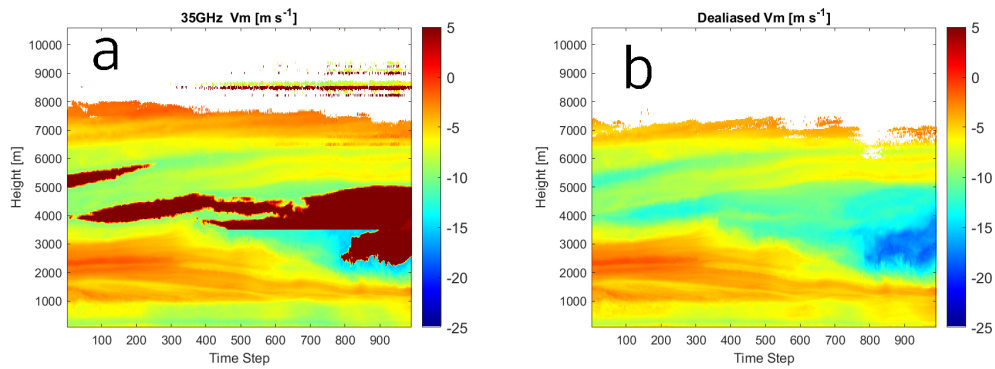


**Figure A.14:**  $V_m$  from 13:00 to 14:00 on 3rd February, 2021. (a) 35GHz LV1 products MDV profile. (b) Dealiased 94GHz MDV profile.

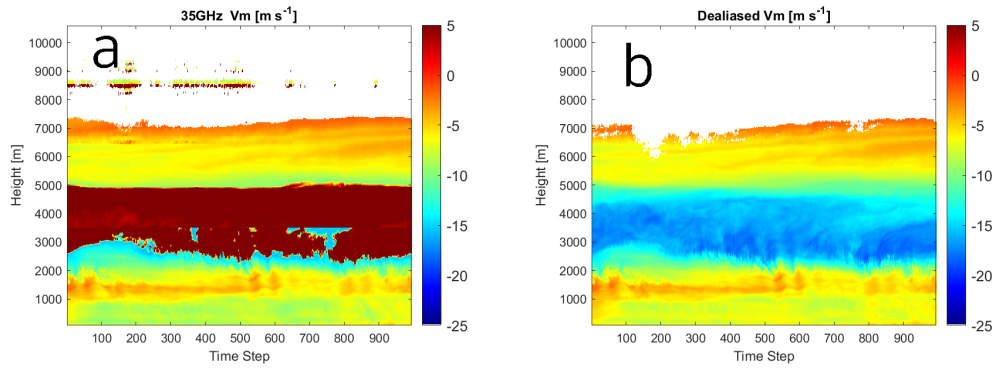


**Figure A.15:**  $V_m$  from 14:00 to 15:00 on 3rd February, 2021. (a) 35GHz LV1 products MDV profile. (b) Dealiased 94GHz MDV profile.

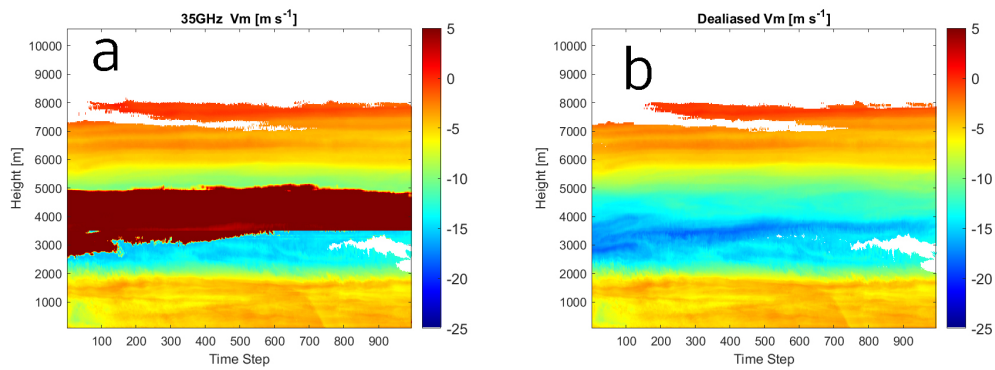


**Figure A.16:**  $V_m$  from 15:00 to 16:00 on 3rd February, 2021. (a) 35GHz LV1 products MDV profile. (b) Dealiased 94GHz MDV profile.

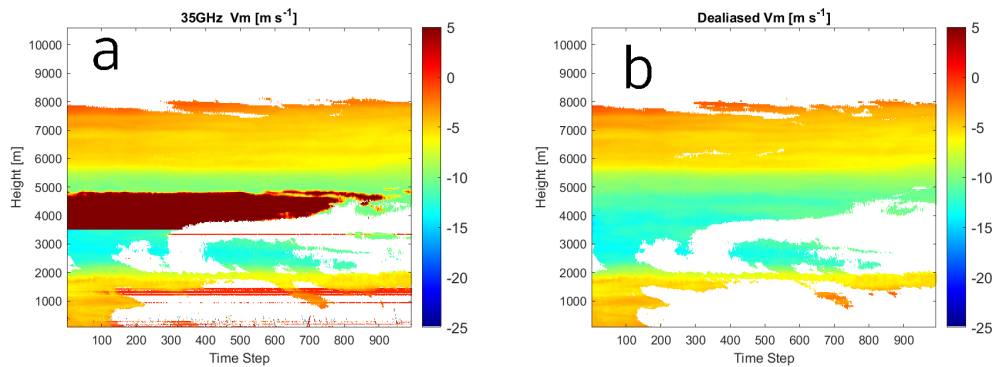


**Figure A.17:**  $V_m$  from 16:00 to 17:00 on 3rd February, 2021. (a) 35GHz LV1 products MDV profile. (b) Dealiased 94GHz MDV profile.

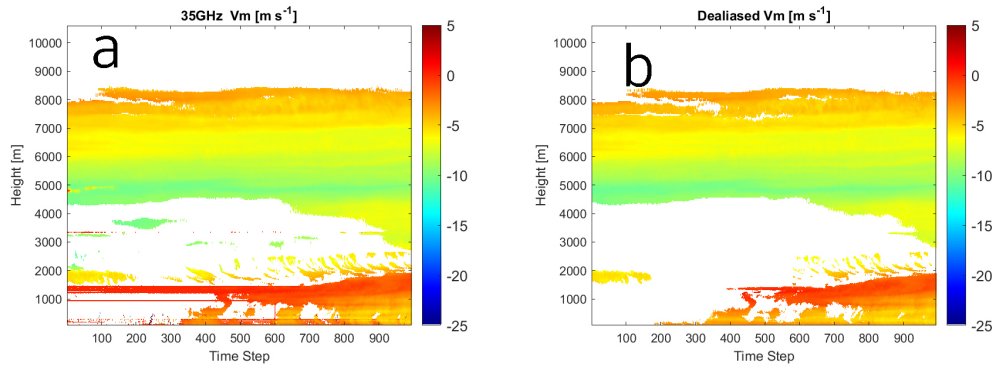


**Figure A.18:**  $V_m$  from 17:00 to 18:00 on 3rd February, 2021. (a) 35GHz LV1 products MDV profile. (b) Dealiased 94GHz MDV profile.

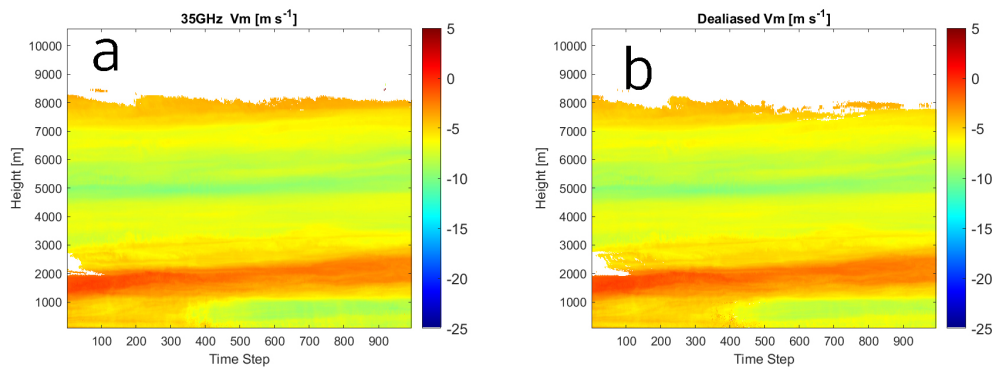


**Figure A.19:**  $V_m$  from 18:00 to 19:00 on 3rd February, 2021. (a) 35GHz LV1 products MDV profile. (b) Dealiased 94GHz MDV profile.

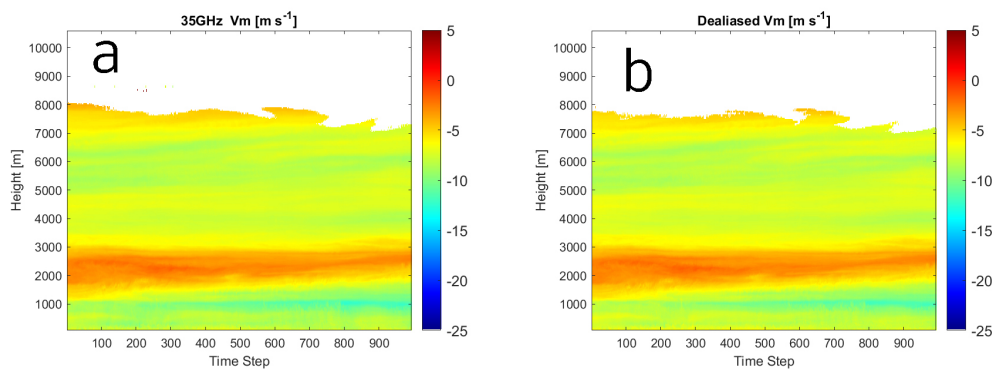


**Figure A.20:**  $V_m$  from 19:00 to 20:00 on 3rd February, 2021. (a) 35GHz LV1 products MDV profile. (b) Dealiased 94GHz MDV profile.

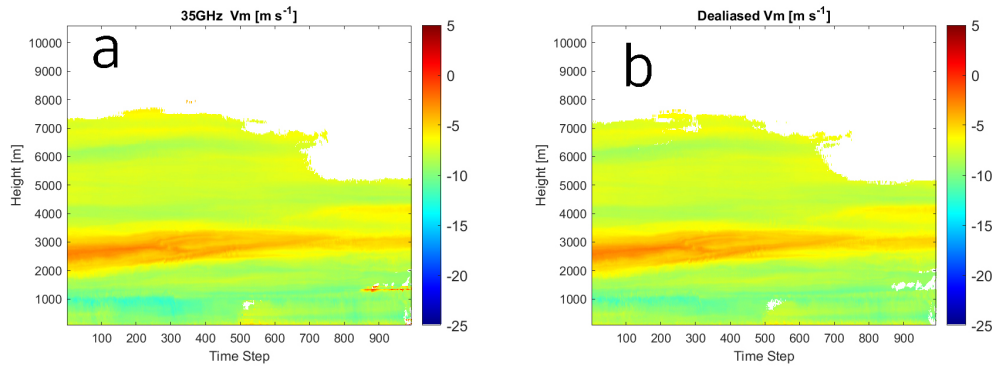


**Figure A.21:**  $V_m$  from 20:00 to 21:00 on 3rd February, 2021. (a) 35GHz LV1 products MDV profile. (b) Dealiased 94GHz MDV profile.

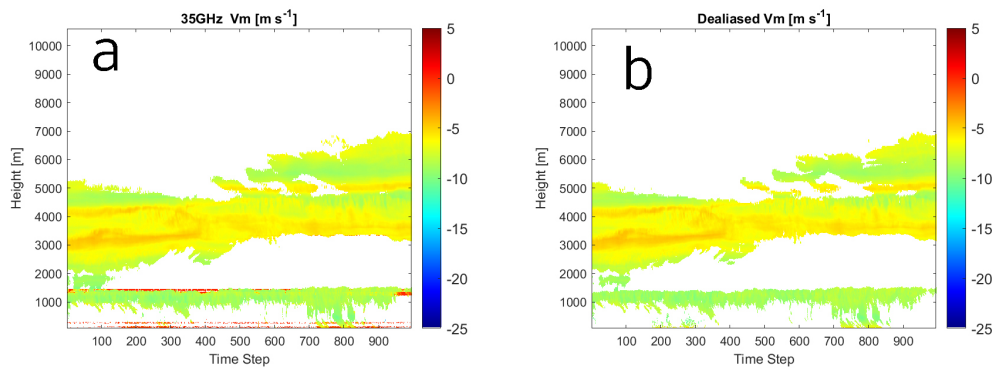


**Figure A.22:**  $V_m$  from 21:00 to 22:00 on 3rd February, 2021. (a) 35GHz LV1 products MDV profile. (b) Dealiased 94GHz MDV profile.

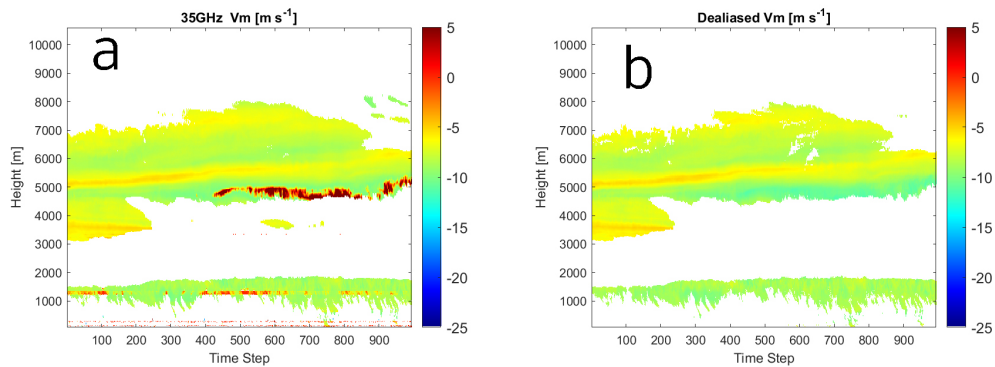


**Figure A.23:**  $V_m$  from 22:00 to 23:00 on 3rd February, 2021. (a) 35GHz LV1 products MDV profile. (b) Dealiased 94GHz MDV profile.

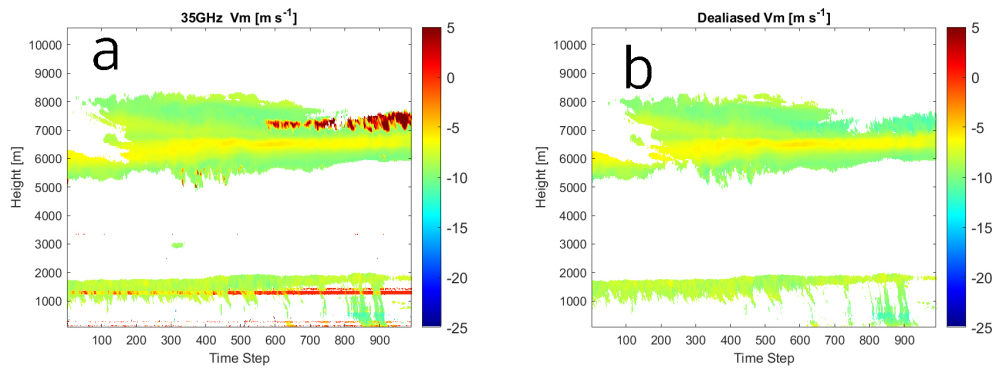


**Figure A.24:**  $V_m$  from 23:00 to 24:00 on 3rd February, 2021. (a) 35GHz LV1 products MDV profile. (b) Dealiased 94GHz MDV profile.

# B

## All dealiased $V_m$ on 18th June, 2021

All 24 hours of dealiased  $V_m$  profiles on 18th June, 2021 are shown below. For comparison, the original  $V_m$  profiles of 35GHz LV1 products are also provided.

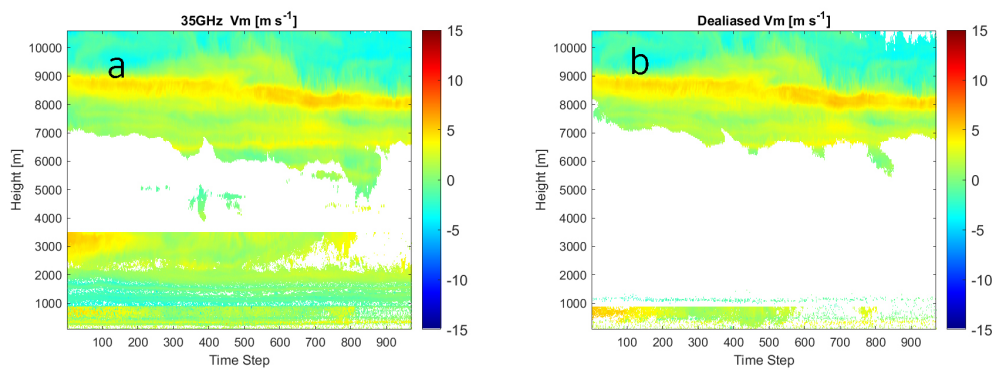


**Figure B.1:**  $V_m$  from 00:00 to 01:00 on 18th June, 2021 (a) 35GHz LV1 products MDV profile. (b) Dealiased 94GHz MDV profile.

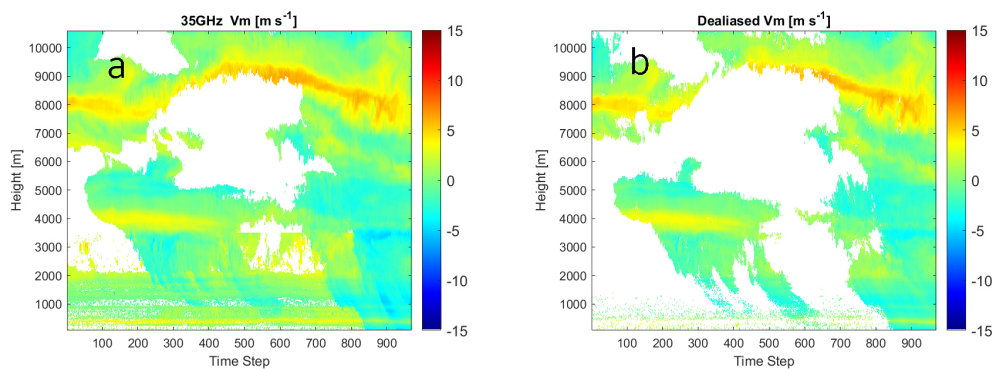


**Figure B.2:**  $V_m$  from 01:00 to 02:00 on 18th June, 2021 (a) 35GHz LV1 products MDV profile. (b) Dealiased 94GHz MDV profile.

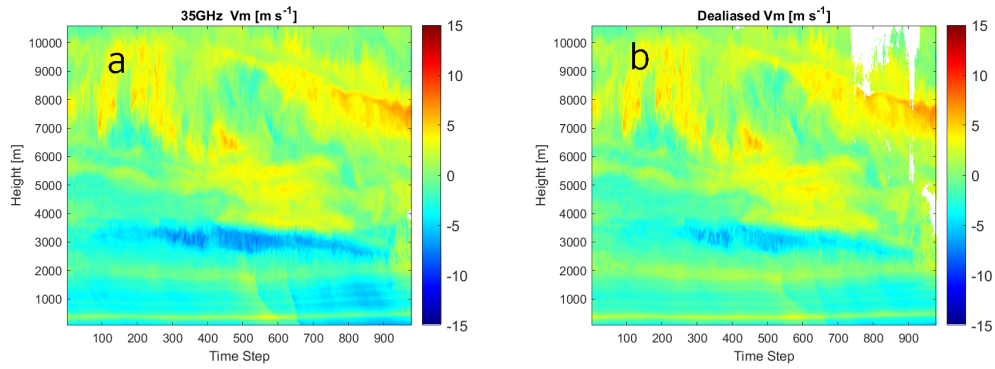


**Figure B.3:**  $V_m$  from 02:00 to 03:00 on 18th June, 2021 (a) 35GHz LV1 products MDV profile. (b) Dealiased 94GHz MDV profile.

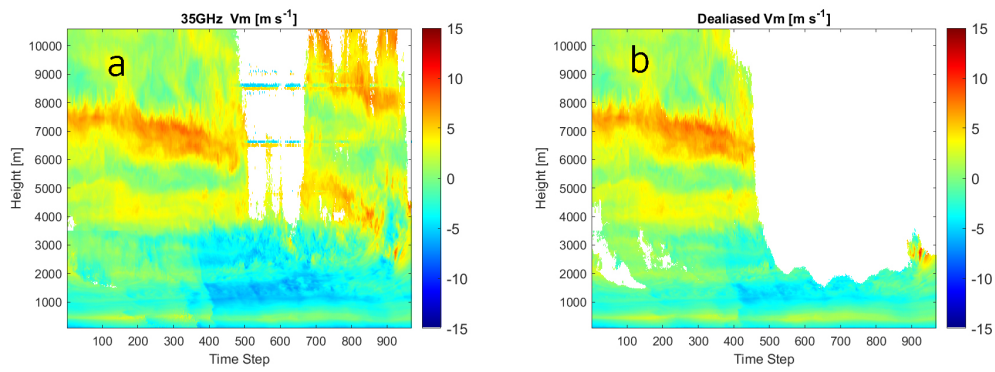


**Figure B.4:**  $V_m$  from 03:00 to 04:00 on 18th June, 2021 (a) 35GHz LV1 products MDV profile. (b) Dealiased 94GHz MDV profile.

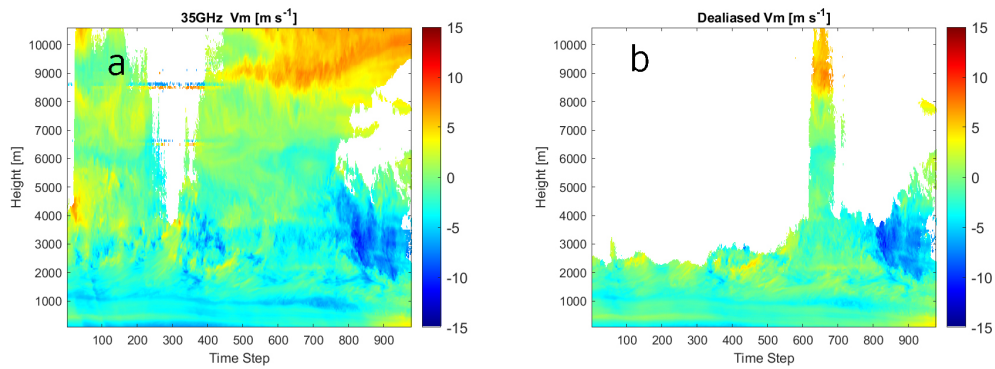


**Figure B.5:**  $V_m$  from 04:00 to 05:00 on 18th June, 2021 (a) 35GHz LV1 products MDV profile. (b) Dealiased 94GHz MDV profile.

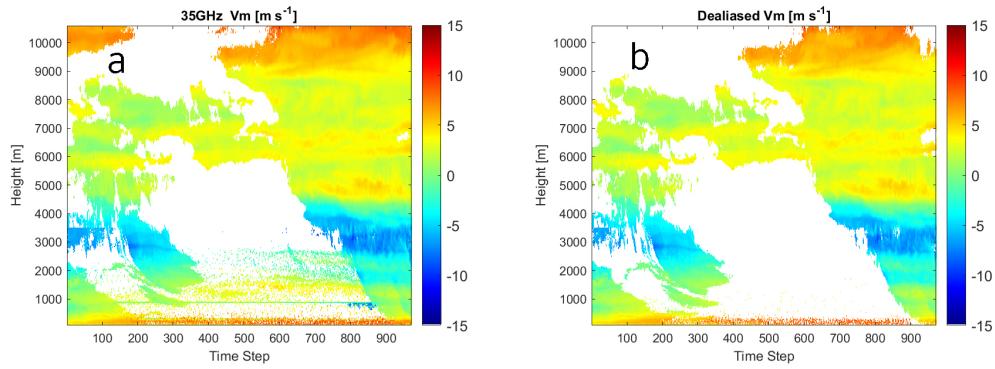


**Figure B.6:**  $V_m$  from 05:00 to 06:00 on 18th June, 2021 (a) 35GHz LV1 products MDV profile. (b) Dealiased 94GHz MDV profile.

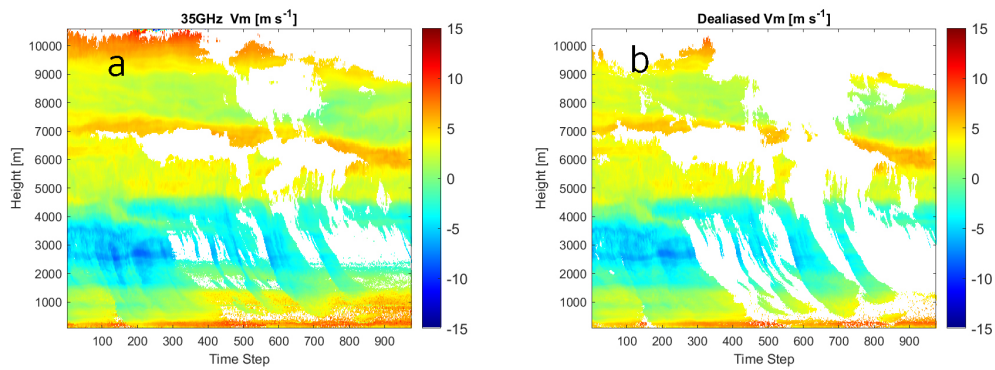


**Figure B.7:**  $V_m$  from 06:00 to 07:00 on 18th June, 2021 (a) 35GHz LV1 products MDV profile. (b) Dealiased 94GHz MDV profile.

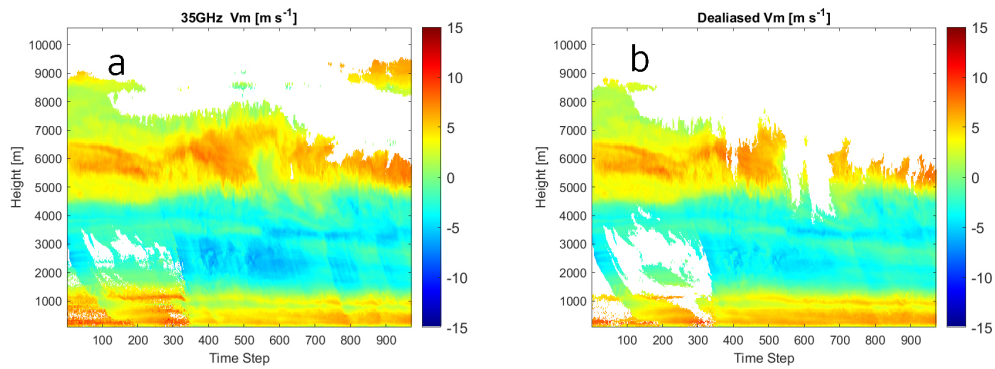


**Figure B.8:**  $V_m$  from 07:00 to 08:00 on 18th June, 2021 (a) 35GHz LV1 products MDV profile. (b) Dealiased 94GHz MDV profile.

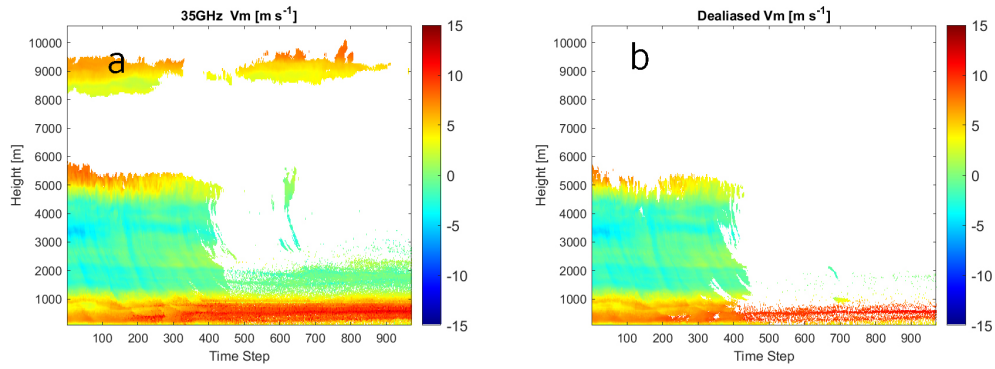


**Figure B.9:**  $V_m$  from 08:00 to 09:00 on 18th June, 2021 (a) 35GHz LV1 products MDV profile. (b) Dealiased 94GHz MDV profile.

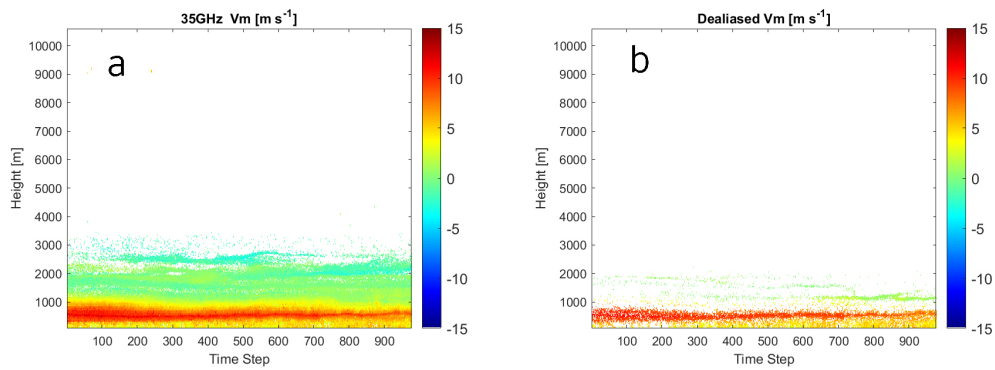


**Figure B.10:**  $V_m$  from 09:00 to 10:00 on 18th June, 2021 (a) 35GHz LV1 products MDV profile. (b) Dealiased 94GHz MDV profile.

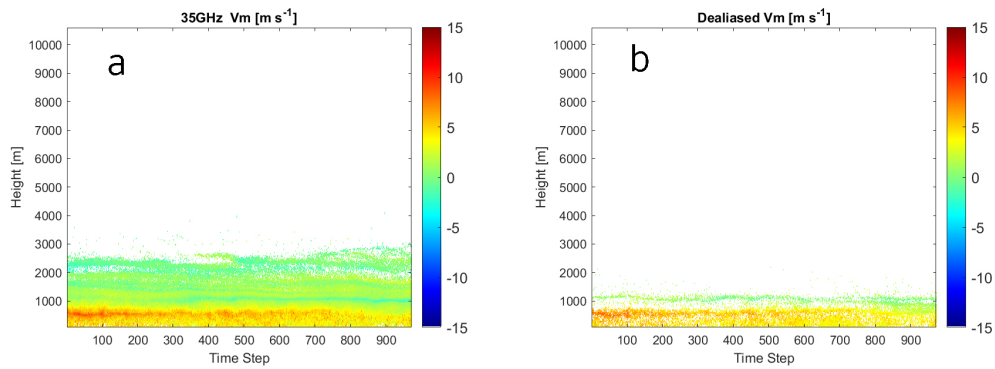


**Figure B.11:**  $V_m$  from 10:00 to 11:00 on 18th June, 2021 (a) 35GHz LV1 products MDV profile. (b) Dealiased 94GHz MDV profile.

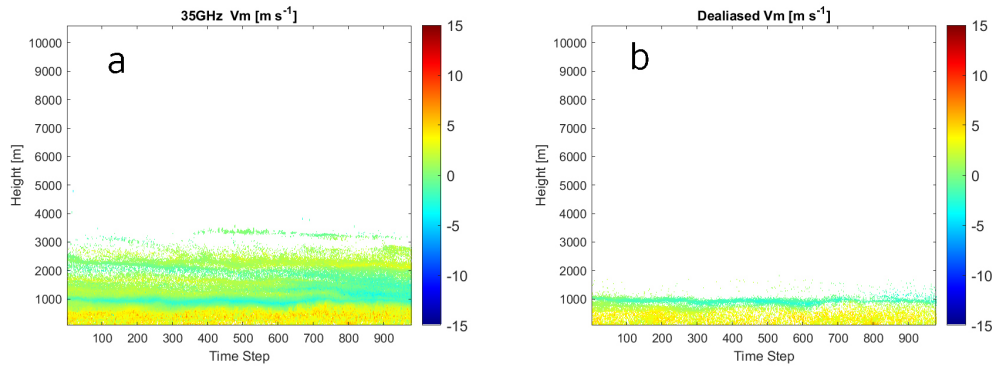


**Figure B.12:**  $V_m$  from 11:00 to 12:00 on 18th June, 2021 (a) 35GHz LV1 products MDV profile. (b) Dealiased 94GHz MDV profile.

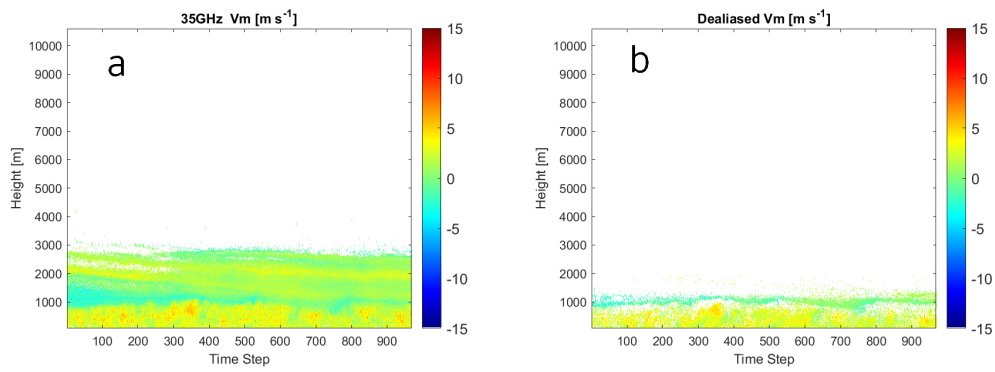


**Figure B.13:**  $V_m$  from 12:00 to 13:00 on 18th June, 2021 (a) 35GHz LV1 products MDV profile. (b) Dealiased 94GHz MDV profile.

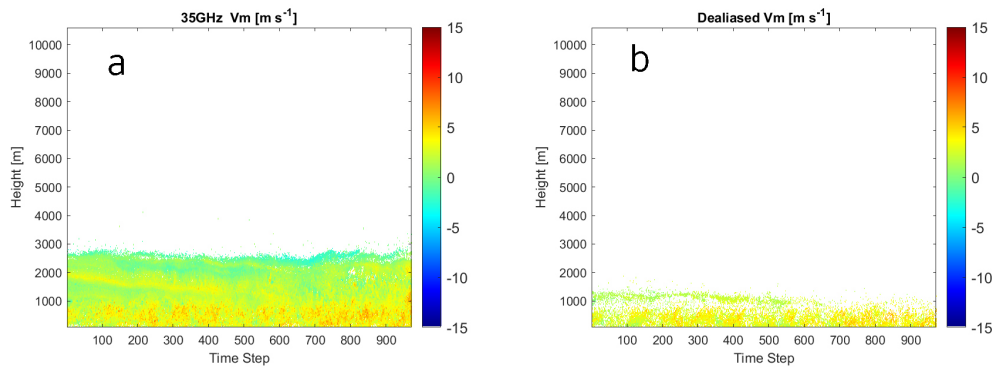


**Figure B.14:**  $V_m$  from 13:00 to 14:00 on 18th June, 2021 (a) 35GHz LV1 products MDV profile. (b) Dealiased 94GHz MDV profile.

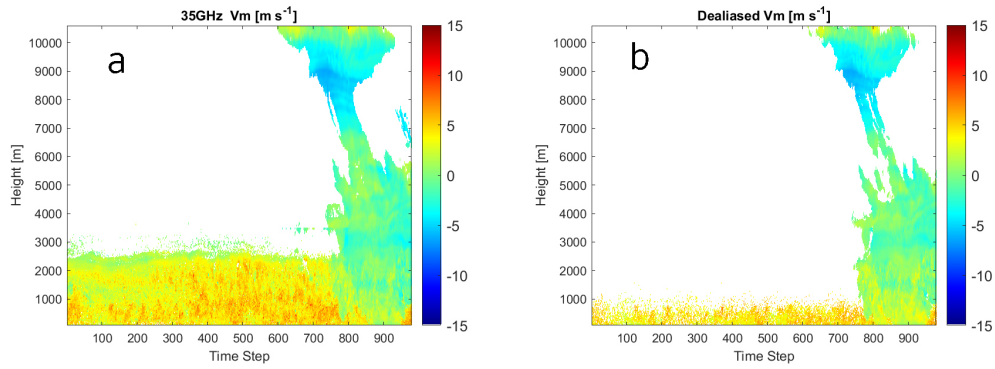


**Figure B.15:**  $V_m$  from 14:00 to 15:00 on 18th June, 2021 (a) 35GHz LV1 products MDV profile. (b) Dealiased 94GHz MDV profile.

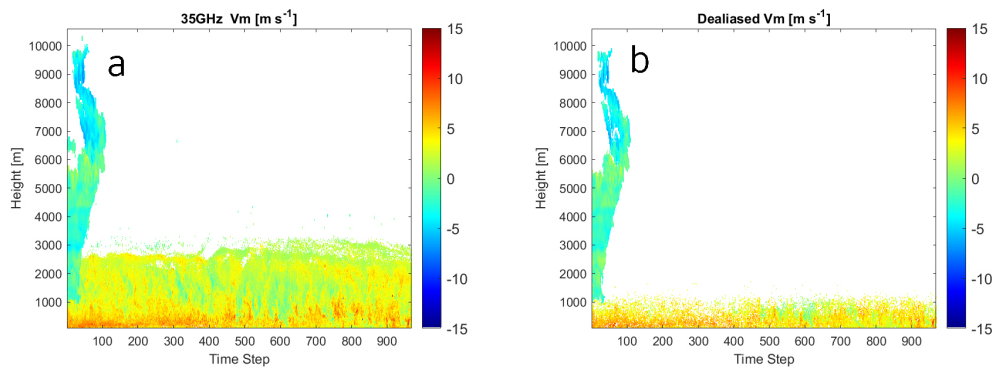


**Figure B.16:**  $V_m$  from 15:00 to 16:00 on 18th June, 2021 (a) 35GHz LV1 products MDV profile. (b) Dealiased 94GHz MDV profile.

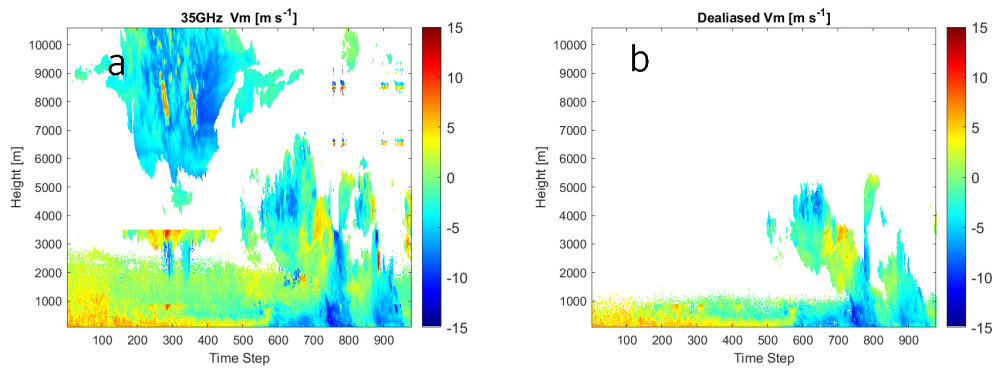


**Figure B.17:**  $V_m$  from 16:00 to 17:00 on 18th June, 2021 (a) 35GHz LV1 products MDV profile. (b) Dealiased 94GHz MDV profile.

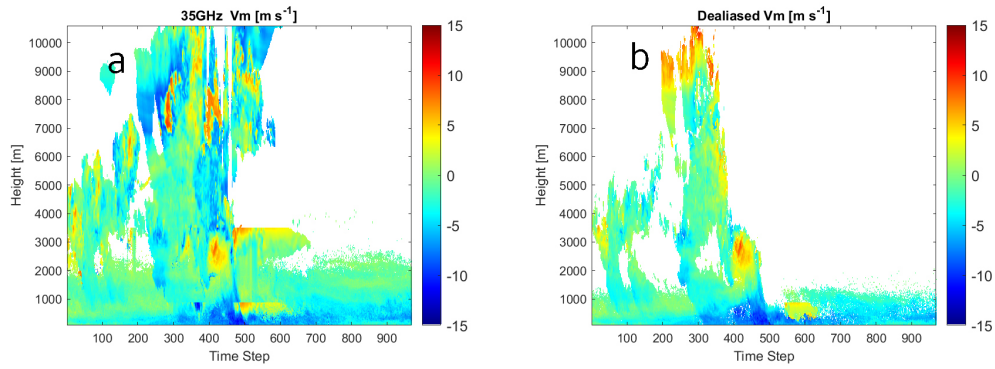


**Figure B.18:**  $V_m$  from 17:00 to 18:00 on 18th June, 2021 (a) 35GHz LV1 products MDV profile. (b) Dealiased 94GHz MDV profile.

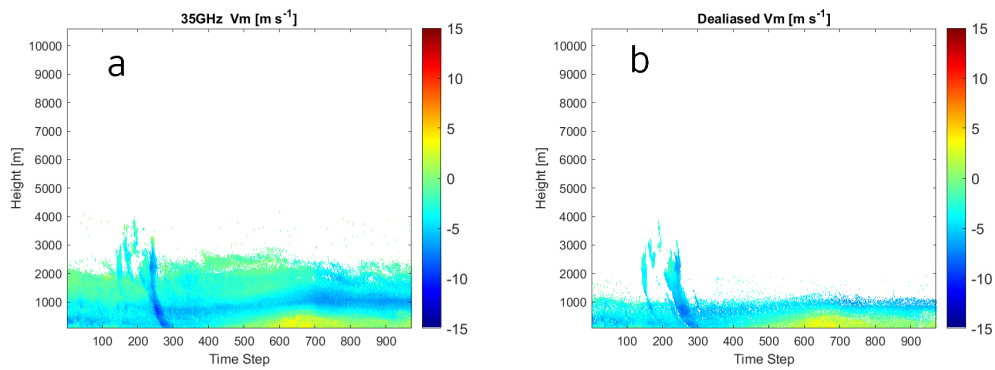


**Figure B.19:**  $V_m$  from 18:00 to 19:00 on 18th June, 2021 (a) 35GHz LV1 products MDV profile. (b) Dealiased 94GHz MDV profile.

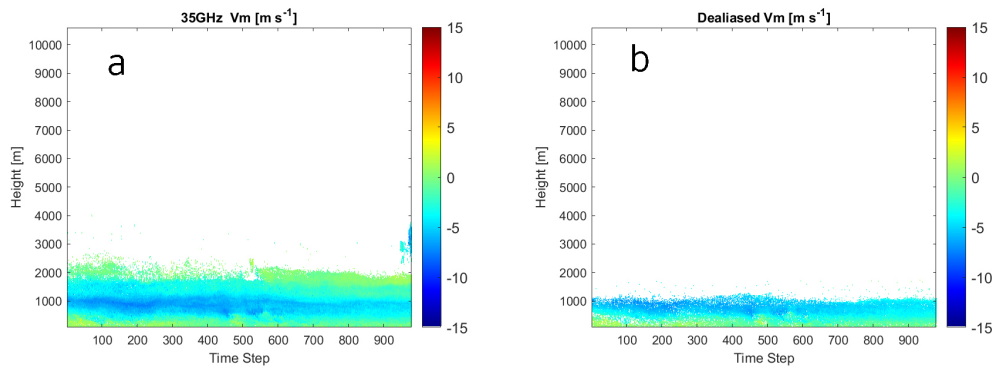


**Figure B.20:**  $V_m$  from 19:00 to 20:00 on 18th June, 2021 (a) 35GHz LV1 products MDV profile. (b) Dealiased 94GHz MDV profile.

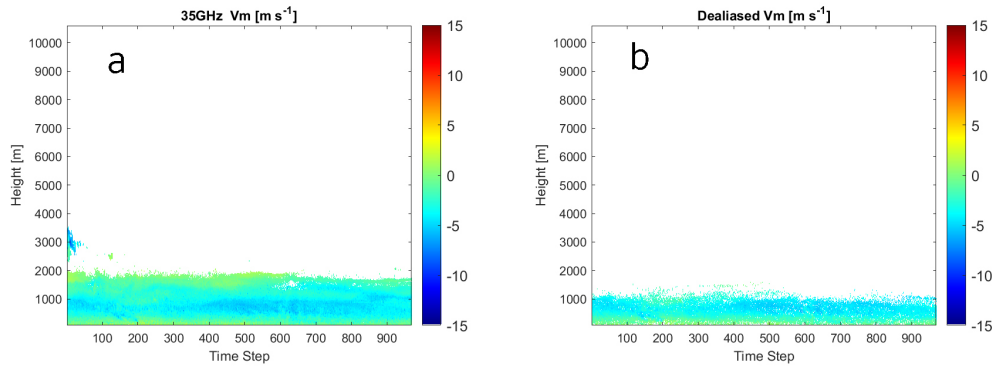


**Figure B.21:**  $V_m$  from 20:00 to 21:00 on 18th June, 2021 (a) 35GHz LV1 products MDV profile. (b) Dealiased 94GHz MDV profile.

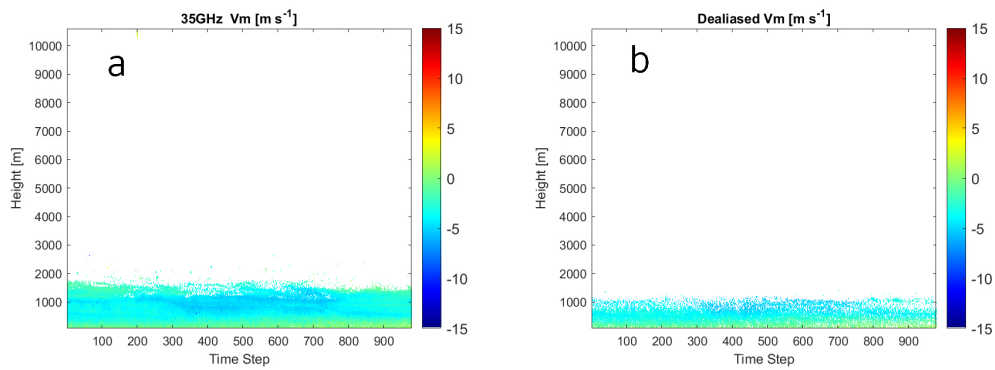


**Figure B.22:**  $V_m$  from 21:00 to 22:00 on 18th June, 2021 (a) 35GHz LV1 products MDV profile. (b) Dealiased 94GHz MDV profile.

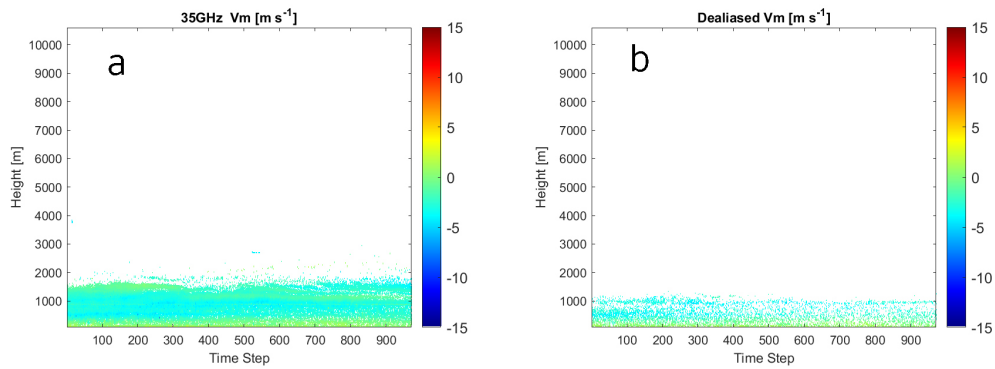


**Figure B.23:**  $V_m$  from 22:00 to 23:00 on 18th June, 2021 (a) 35GHz LV1 products MDV profile. (b) Dealiased 94GHz MDV profile.

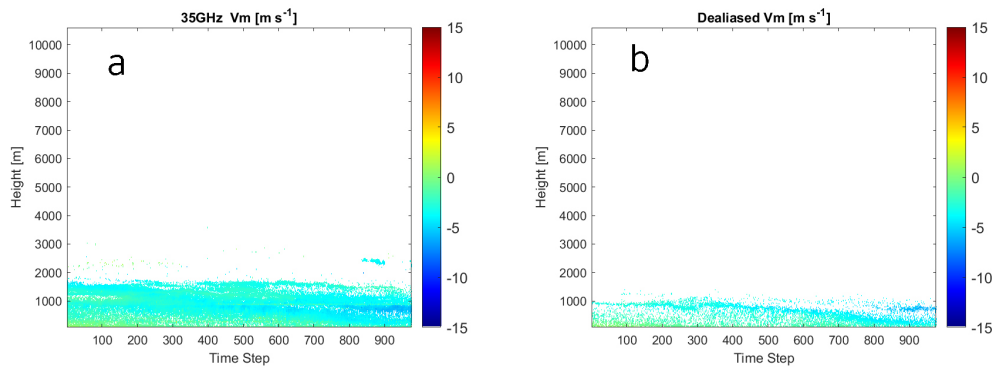
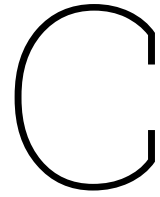


**Figure B.24:**  $V_m$  from 23:00 to 24:00 on 18th June, 2021 (a) 35GHz LV1 products MDV profile. (b) Dealiased 94GHz MDV profile.



# Inputs and Outputs of the code

The inputs and outputs of the algorithm are shown in tables below:

HSpec (VSpec)	The Doppler spectra in LV0 product.
C1RHV	Correlation coefficient profile of Chirp 1 in LV1 product.
SurfWD	Measured surface wind direction
SurfWS	Measured surface wind speed
Azm	Radar azimuth direction
Elv	Radar elevation angle
MaxVel	Maximum Doppler velocity
Range	Radar range of all bins

**Table C.1:** Input data

C1,C2,C3	Original spectra data in Chirp 1,2,3
c1,c2,c3	Dealiased spectra in Chirp 1,2,3
vd_all	Dealiased mean Doppler velocity profile
vmin	The start velocity of dealiased spectra

**Table C.2:** Output data

More details can be found in the comments in the code.